

Fast Queries of Fibered Barcodes

Michael Lesnick*

Matthew Wright†

Abstract

The *fibered barcode* $\mathcal{F}(M)$ of a bipersistence module M is the map sending each non-negatively sloped affine line $\ell \subset \mathbb{R}^2$ to the barcode of the restriction of M along ℓ . The simplicity, computability, and stability of $\mathcal{F}(M)$ make it a natural choice of invariant for data analysis applications. In an earlier preprint [79], we introduced a framework for real-time interactive visualization of $\mathcal{F}(M)$, which allows the user to select a single line ℓ via a GUI and then plots the associated barcode. This visualization is a key feature of our software RIVET for the visualization and analysis of bipersistent homology. Such interactive visualization requires a framework for efficient queries of $\mathcal{F}(M)$, i.e., for quickly obtaining the barcode along a given line ℓ . To enable such queries, we introduced a novel data structure based on planar line arrangements, called an *augmented arrangement*. The aim of the present paper is to give an updated and improved exposition of the parts of [79] concerning the mathematics of the augmented arrangement and its computation. Notably, by taking the input to be a minimal presentation rather than a chain complex, we are able to substantially simplify our main algorithm and its complexity analysis.

Contents

1	Introduction	2
1.1	Overview	2
1.2	The Fibered Barcode	4
1.3	The Augmented Arrangement	5
1.4	Main Results	7
1.5	Related Work on Multiparameter Persistence	7
1.6	Outline	10
2	Mathematical Preliminaries	10
2.1	Free Persistence Modules and Presentations	10
2.2	Computation of Persistence Barcodes	11
2.3	Updating an RU -Decomposition	12
2.4	Line Arrangements	13

*University at Albany, Albany, NY, USA; mlesnick@albany.edu

†St. Olaf College, Northfield, MN, USA; wright5@stolaf.edu

3	The Augmented Arrangement	14
3.1	Definition of the Line Arrangement	15
3.2	Push Maps	16
3.3	Barcode Templates	18
4	Querying the Augmented Arrangement	20
4.1	The Query Procedure	20
4.2	Correctness of the Query Procedure	21
4.3	Computational Details and Complexity of Queries	24
5	Computing the Augmented Arrangement	25
5.1	Computing the Barcode Templates	26
5.2	Updating the Template Points and Lift Map	27
5.3	Permuting Matrices and Updating the RU -Decomposition	31
5.4	Implementation Details	32
5.5	Computing a Walk Through the Faces	33
6	Complexity of Computing the Augmented Arrangement	34

1 Introduction

1.1 Overview

Topological data analysis (TDA) studies the shape of data using tools from algebraic topology. Persistent homology, one of the central tools of TDA, provides invariants of data called barcodes by constructing a filtration of topological spaces from the data, taking homology with coefficients in a field, and applying a standard structure theorem to the resulting diagram of vector spaces. In the last 25 years, persistent homology has been used in hundreds of applications [64] and has been the subject of extensive theoretical work. Introductions can be found in many textbooks and surveys, e.g., [16, 24, 27, 34, 55, 57, 89, 94, 104].

For many data types, such as noisy point cloud data, a single filtered space does not adequately encode the structure of interest in our data [25, 28, 33]. This motivates the consideration of multiparameter persistent homology [28, 62], which begins with the construction of a *multiparameter filtration*. For algebraic reasons, defining barcodes in the multiparameter setting is problematic. This creates significant challenges for the theoretical and practical development of multiparameter persistent homology. In recent years, there has been a surge in effort on these challenges, leading to substantial progress in theory, computation, and software; see Section 1.5 for a brief overview of some of this work, and [18] for a detailed introduction.

Visualization plays a major role in applications of persistent homology, but is more challenging in the multiparameter setting than in the 1-parameter setting. In 2015, we posted a preprint [79] which introduced a novel framework for the interactive visualization of bipersistent homology (i.e., 2-parameter persistent homology). This framework is implemented in the software RIVET [100], which was the first publicly available software for analysis and visualization of bipersistence. To elaborate, RIVET implements algorithms for several computational problems in the bipersistence pipeline. Specifically, RIVET computes

- function-Rips and degree-Rips bifiltrations of metric data,
- a minimal presentation of a homology module of a bifiltration, and
- three invariants of such a homology module, namely, the Hilbert function, bigraded Betti numbers, and fibered barcode.

The fibered barcode $\mathcal{F}(M)$ of a bipersistence module M is the map sending each non-negatively sloped affine line $\ell \subset \mathbb{R}^2$ to the barcode of the restriction of M along ℓ ; see Section 1.2. RIVET provides a novel visualization of the three invariants, whose key feature is an interactive scheme for exploring the fibered barcode.

The preprint [79] explained in detail the mathematical and algorithmic foundations of our scheme for visualizing the fibered barcode. The scheme hinges on a framework for efficient queries of the fibered barcode, i.e., for quickly obtaining the barcode along a given line $\ell \subset \mathbb{R}^2$. In [79], we introduced a data structure based on planar line arrangements, called an *augmented arrangement*, on which we can perform such queries. Once the augmented arrangement has been computed, querying it for the barcode along a given line is far more efficient than computing the barcode from scratch. On typical input, queries of our data structure in RIVET are fast enough to enable smooth animations of the changing barcode as the query line ℓ is varied by the user. Moreover, the cost of computing and storing the augmented arrangement is small enough for practical use. See Theorems 1.2 and 1.3 below for complexity bounds.

The isomorphism type of a bipersistence module M can be efficiently encoded in a *minimal presentation*. Concretely, this is a matrix with an \mathbb{R}^2 -valued label for each row and each column, where the labels of the rows and columns give the 0th and 1st bigraded Betti numbers of M , respectively; see Section 2.1. Notably, early versions of RIVET did not compute minimal presentations, and instead computed augmented arrangements directly from the chain complexes of bifiltrations. The augmented arrangement computation detailed in [79] closely parallels what was implemented in the early versions of RIVET, and thus also does not exploit minimal presentations.

In subsequent work [80], we introduced a novel algorithm for computing minimal presentations of bipersistence modules and implemented this in RIVET. This algorithm runs in cubic time and quadratic space, and is asymptotically more memory efficient than a classical approach based on Schreyer’s algorithm. Computational experiments reported in [80] showed that RIVET’s minimal presentation computations are much faster and more scalable than comparable computations in standard open-source commutative algebra software.

Several subsequent works have revisited the problem of computing minimal presentations for bipersistent homology, leading to further improvements: Kerber and Rolle introduced an optimized version of the algorithm from [80] that performs far better in practice [63, 69]; Bauer et al. developed a cohomological approach that is optimized for *function–Rips bifiltrations* [6]; and most recently, Morozov and Scoccola gave a specialized algorithm for the case of 0th homology, which runs in nearly linear time [87].

It turns out that our algorithm from [79] for computing the augmented arrangement admits major simplifications if the input is assumed to be a minimal presentation rather than a chain complex. These simplifications have not previously appeared in print. Moreover, first computing a minimal presentation typically leads to drastic speedups to RIVET’s augmented arrangement computation, partly because the chain complexes are typically far larger than the minimal presentations of their homology.

With this in mind, our aim in this paper is to present a more concise and polished exposition of the scheme from [79] for fast queries of fibered barcodes, assuming that the input is a minimal presentation. This paper mostly supersedes the mathematical core of [79], but does not replace the material from [79] on visualization and software. Some updates of such material from [79] can be found in the RIVET documentation [100].

In what follows, we define the fibered barcode, give a high-level introduction to the augmented arrangement, and state the main results of this paper, which are variants of [79, Theorems 1.3 and 1.4], respectively.

1.2 The Fibered Barcode

We prepare for definition of fibered barcodes by introducing some notation and definitions; additional background will be covered in Section 2. Let \mathbf{Vec} denote the category of vector spaces over a fixed field \mathbf{k} . We regard a poset \mathbb{P} as a category with object set \mathbb{P} and morphisms the relations $p \leq q$. Define a (\mathbb{P} -indexed) *persistence module* to be a functor $M: \mathbb{P} \rightarrow \mathbf{Vec}$ for some poset \mathbb{P} . Thus, M consists of a vector space M_p for each $p \in \mathbb{P}$, together with a linear map $M_{p,q}$ for each $p \leq q \in \mathbb{P}$, such that $M_{p,r} = M_{q,r} \circ M_{p,q}$ for all $p \leq q \leq r$. We say M is *pointwise finite dimensional (p.f.d.)* if $\dim M_p < \infty$ for all $p \in \mathbb{P}$. If \mathbb{P} is totally ordered, then we call M a *1-parameter persistence module*, and if $\mathbb{P} = \mathbb{R}^2$ with the usual product partial order (i.e., $(a_1, a_2) \leq (b_1, b_2)$ if and only if $a_1 \leq b_1$ and $a_2 \leq b_2$), then we call M a *bipersistence module*.

An *interval* I in a totally ordered set \mathbb{T} is a non-empty subset I such that whenever $r < s < t \in \mathbb{T}$ and $r, t \in I$, we also have $s \in I$. We regard $\mathbb{T} \sqcup \{\infty\}$ as poset with $t < \infty$ for all $t \in \mathbb{T}$. Given $s < t \in \mathbb{T} \sqcup \{\infty\}$, let $[s, t) \subset \mathbb{T}$ be the interval

$$[s, t) = \{x \in \mathbb{T} \mid s \leq x < t\}.$$

According to a standard structure theorem for persistence modules, for any totally ordered set \mathbb{T} and p.f.d. 1-parameter persistence module $M: \mathbb{T} \rightarrow \mathbf{Vec}$, M decomposes in

an essentially unique way into indecomposables, where the isomorphism classes of the indecomposables are parameterized by intervals in \mathbb{T} [50, 109]. This yields a multiset $\mathcal{B}(M)$ of intervals in \mathbb{T} called the *barcode* of M , which determines M up to isomorphism. If M is finitely presented (see Section 2.1) then it is p.f.d., and each interval of $\mathcal{B}(M)$ is of the form $[s, t)$.

We now formally define the fibered barcode of a p.f.d. bipersistence module M . For $\ell \subset \mathbb{R}^2$ an affine line with non-negative slope, we let $M^\ell : \ell \rightarrow \mathbf{Vec}$ denote the restriction of M to ℓ . As the restriction of the partial order on \mathbb{R}^2 to ℓ is a total order, M^ℓ has a well-defined *barcode* $\mathcal{B}(M^\ell)$, which is a multiset of intervals in ℓ . We call the map $\ell \mapsto \mathcal{B}(M^\ell)$ the *fibered barcode* of M , and denote it as $\mathcal{F}(M)$. Fibered barcodes were introduced in [30], and this name for them was introduced in [79]. As observed in [30], $\mathcal{F}(M)$ is equivalent to the *rank invariant* of M [28], i.e., the map $(a \leq b) \mapsto \text{rank } M_{a,b}$.

Remark 1.1. The fibered barcode $\mathcal{F}(M)$ satisfies two natural stability properties, which we call *internal stability* and *external stability*. In brief, internal stability [9, 75] says that at lines $\ell \subset \mathbb{R}^2$ of positive, finite slope, the barcode $\mathcal{B}(M^\ell)$ is continuous with respect to perturbations of ℓ ; see [75] for a precise quantitative statement. External stability [30, 75] is the inequality

$$d_m(\mathcal{F}(M), \mathcal{F}(N)) \leq d_I(M, N),$$

where d_I is the *interleaving distance* on bipersistence modules [76] and d_m is the *matching distance* on fibered barcodes [30]. For p.f.d. bipersistence modules M and N , d_m is defined by

$$d_m(\mathcal{F}(M), \mathcal{F}(N)) = \sup_{\ell} w_{\ell} \cdot d_b(\mathcal{B}(M^\ell), \mathcal{B}(N^\ell)),$$

where ℓ ranges over affine lines in \mathbb{R}^2 of positive, finite slope, d_b is the *bottleneck distance* on barcodes [43] (whose usual definition over \mathbb{R} extends to ℓ because \mathbb{R} and ℓ are isometric), and for s_{ℓ} the slope of ℓ ,

$$w_{\ell} = \begin{cases} \frac{1}{\sqrt{1+s_{\ell}^2}} & \text{if } s_{\ell} \geq 1, \\ \frac{1}{\sqrt{1+\frac{1}{s_{\ell}^2}}} & \text{if } s_{\ell} < 1. \end{cases}$$

1.3 The Augmented Arrangement

Now let M be a finitely presented bipersistence module. We let $\mathcal{A}^{\bullet}(M)$ denote the *augmented arrangement* of M , the data structure underlying our scheme for fast queries of $\mathcal{F}(M)$. It consists of three parts:

1. a line arrangement $\mathcal{A}(M)$ in $[0, \infty) \times \mathbb{R}$ (i.e., a cell decomposition induced by a set of intersecting lines),
2. for each face (i.e., 2-cell) Δ of $\mathcal{A}(M)$, a collection \mathcal{B}^{Δ} of pairs $(a, b) \in \mathbb{R}^2 \times (\mathbb{R}^2 \cup \infty)$, called the *barcode template* at Δ , and

3. a search data structure for performing log-time point location queries in $\mathcal{A}(M)$.

We give the definition of $\mathcal{A}^\bullet(M)$ in Section 3. Here, to convey the flavor of the definition, we briefly mention a few key ideas underlying the construction. The line arrangement $\mathcal{A}(M)$ is formed by dual lines of certain joins of elements in the union of the support of the 0th and 1st Betti numbers of M . Each barcode template \mathcal{B}^Δ is (up to a canonical bijection) the barcode of the restriction of M to a finite, totally ordered subset of \mathbb{R}^2 . As discussed in Section 2.4, search data structures for log-time point location in line arrangements are standard objects in computational geometry; we take the search data structure of $\mathcal{A}^\bullet(M)$ to be a standard one.

We next briefly describe how we query $\mathcal{A}^\bullet(M)$ for the barcodes $\mathcal{B}(M^\ell)$. A standard point-line duality, described in Section 3.1, parameterizes the set of affine lines in \mathbb{R}^2 with non-negative, finite slope by $[0, \infty) \times \mathbb{R}$. For simplicity, here we restrict attention to the generic case where the dual of ℓ lies in a face Δ of $\mathcal{A}(M)$; the general case is similar and is treated in Section 4.

To obtain $\mathcal{B}(M^\ell)$, for each pair $(a, b) \in \mathcal{B}^\Delta$, we “push” both a and b either upward or rightward onto the line ℓ , as illustrated in Fig. 1. This gives a pair of points $\text{push}_\ell(a), \text{push}_\ell(b) \in \ell$. We take $\text{push}_\ell(\infty) = \infty$. See Section 3.2 for the formal definition of the map push_ℓ . Theorem 4.2 says that

$$\mathcal{B}(M^\ell) = \{ [\text{push}_\ell(a), \text{push}_\ell(b)] \mid (a, b) \in \mathcal{B}^\Delta \},$$

where $[\text{push}_\ell(a), \text{push}_\ell(b)]$ is understood to be an interval in ℓ . Thus, to obtain the barcode of $\mathcal{B}(M^\ell)$ it suffices to identify the face Δ via a point location query and then compute $\text{push}_\ell(a)$ and $\text{push}_\ell(b)$ for each $(a, b) \in \mathcal{B}^\Delta$.

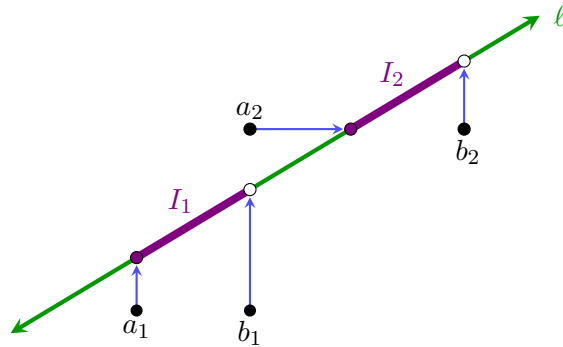


Figure 1: The barcode $\mathcal{B}(M^\ell)$ is obtained from the barcode template \mathcal{B}^Δ by “pushing” the points of each pair onto ℓ . In this example, $\mathcal{B}^\Delta = \{(a_1, b_1), (a_2, b_2)\}$, and $\mathcal{B}(M^\ell)$ consists of two disjoint intervals I_1, I_2 .

1.4 Main Results

We now state our two main theorems, which bound the cost of computing, storing, and querying $\mathcal{A}^\bullet(M)$. As is standard in computational geometry, we adopt the *real RAM* model of computation, where arithmetic operations over the reals require constant time [93]. We also assume that all elementary arithmetic operations in the field \mathbf{k} require constant time. In TDA, most homology computations are done over finite fields, where the latter assumption holds.

Let $\kappa = \kappa_x \cdot \kappa_y$, where κ_x and κ_y are the number of unique x and y coordinates, respectively, of points in the union of the supports of the 0th and 1st bigraded Betti numbers of M ; see Section 2.1.

Theorem 1.2. *Given a minimal presentation η of M with a total of m rows and columns,*

- (i) $\mathcal{A}^\bullet(M)$ has size $O(m\kappa^2)$,
- (ii) We can compute $\mathcal{A}^\bullet(M)$ from η in $O(m^3\kappa + \kappa^2(m + \log \kappa))$ time and $O(m^2 + m\kappa^2)$ memory.

Theorem 1.3.

- (i) For a line ℓ whose dual lies in a face of $\mathcal{A}(M)$, we can query $\mathcal{A}^\bullet(M)$ for $\mathcal{B}(M^\ell)$ in time $O(\log \kappa + |\mathcal{B}(M^\ell)|)$, where $|\mathcal{B}(M^\ell)|$ denotes the number of intervals in $\mathcal{B}(M^\ell)$.
- (ii) For all other non-negatively sloped lines ℓ , we can query $\mathcal{A}^\bullet(M)$ for $\mathcal{B}(M^\ell)$ in time $O(\log \kappa + |\mathcal{B}(M^{\ell'})|)$, for ℓ' some arbitrarily small perturbation of ℓ .

Theorems 1.2 (i), 1.2 (ii), and 1.3 are proven in Sections 3.3, 6, and 4.3, respectively.

Remark 1.4. In the worst case, $|\kappa| = O(m^2)$. Thus, the size and time to compute $\mathcal{A}^\bullet(M)$ are both $O(m^5)$. To control the cost of computing and storing $\mathcal{A}^\bullet(M)$, we can approximate M by a module M' for which κ is a small constant, by snapping the grades of generators and relations onto a grid. If this snapping changes each coordinate of each generator or relation by at most δ , then we have

$$d_m(\mathcal{F}(M), \mathcal{F}(M')) \leq d_I(M, M') \leq \delta.$$

Thus, $\mathcal{F}(M')$ is a δ -approximation of $\mathcal{F}(M)$ in the matching distance.

1.5 Related Work on Multiparameter Persistence

The computational study of (multi)graded modules over polynomial rings via Gröbner bases has a long history, e.g., see [49, 72, 73, 74]. To our knowledge, the three earliest TDA works to study the algorithmic aspects of multiparameter persistent homology were: a 2009 paper by Carlsson et al. [26], which applied the classical Gröbner basis algorithms

of Buchberger and Schreyer to multiparameter filtrations; a 2011 paper by Cerri et al. [9], which gave an algorithm for the approximate computation of the matching distance on fibered barcodes; and a 2014 paper by Chacholski et al. [32] which studied the problem of expressing the homology of a multiparameter filtration as the homology of a chain complex of free persistence modules. Our previous preprint [79], on RIVET and fast queries of fibered barcodes, seems to have been the fourth TDA paper on algorithmic aspects of multiparameter persistent homology. Since the release of these early papers, research activity in the computational aspects of multiparameter persistence has accelerated significantly, and this is now one of the main areas of research in TDA; see [18] for a recent overview. In what follows, we mention some of the work in this area most closely related to this paper.

Our approach in [79] of using a line arrangement to decompose the space of affine lines in \mathbb{R}^2 has subsequently been used to give the first polynomial-time algorithms to exactly compute the matching distance between fibered barcodes [11, 68]. Fernandes et al. [61] have adapted RIVET’s query scheme to a scheme for querying γ -linear projected barcodes, a different family of barcodes constructed from a multiparameter persistence module. Hickok [66] has also adapted our query scheme to a scheme for querying piecewise-linear families of barcodes indexed by a simplicial complex.

Aspects of RIVET’s visualization of fibered barcodes have been used in Persistable [97], a software for 2-parameter cluster analysis and visualization. Persistable does not implement our fast query scheme or provide real-time interactive updates of barcodes, but instead computes barcodes of 1-parameter slices from scratch. RIVET’s backend for computing fibered barcodes is used in Oliver Vipond’s software for computing multiparameter persistence landscapes (MPLs) [102]; MPL’s are vectorizations of multiparameter persistence modules that are equivalent to the restriction of the fibered barcode to lines of slope one. MPL’s were the first of several vectorizations of multiparameter persistence to be introduced and explored in computations [29, 38, 45, 81, 84]. A software called Multipers [83] implements computational tools for multiparameter persistence introduced in several recent papers [81, 82, 84, 98], and also incorporates code and functionality from many other software packages for multiparameter persistence, including both RIVET and Persistable.

Compared to the theoretical and algorithmic foundations of multiparameter persistence, practical applications of multiparameter persistence are much less developed, though we will expect that this will change as software improves. That said, several papers have explored applications of multiparameter persistence to real data. Two recent publications [8, 103] have applied Vipond’s MPL software to problems in immuno-oncology and spatial transcriptomics. RIVET has also been used to analyze high-dimensional data arising from Wikipedia articles [105], to address the virtual screening problem in computational chemistry [96], and to study molecular generative modules in computational chemistry [96]. Other applications of multiparameter persistence include further work on virtual screening [53], and applications to image analysis [40, 41], time series data [37, 48], polymer prediction [108], structural analysis of biomolecules [106], collection motion of animals [107], and graph representation learning [36]. These applications work with multiparameter per-

sistent homology via very simple algebraic invariants, such as the Hilbert function or the barcodes of coordinate-wise 1-parameter slices.

As noted above, the fibered barcode is equivalent to the rank invariant. Since RIVET was introduced, other works have introduced different representations of (refinements of) the rank invariant. For one example, in the special case of function-Rips bifiltrations of \mathbb{R} -valued functions on finite metric spaces, Cai et al. [23] have defined the *elder-rule-staircase code*, a computable barcode of 0th persistent homology that determines the rank invariant. Besides this, a large body of recent work on multiparameter persistence has studied *signed barcodes* of multiparameter persistence modules. In the 2-parameter case, a signed barcode is a function from a collection of intervals in \mathbb{R}^2 to \mathbb{Z} ; the word *signed* indicates that the function can take negative values. Typically, a signed barcode is equivalent to some other simple invariant, such as the rank invariant or the *generalized rank invariant* [71]; the idea is to encode that invariant in a barcode-like object.

Two main approaches are used to define signed barcodes: Möbius inversion [19, 71] (following ideas of Patel [90]), and relative homological algebra [12, 20, 88] (following ideas of Botnan et al. [19] and Blanchette et al. [13]). In particular, both approaches provide invariants equivalent to the rank invariant [19]. Notably, the *hook signed barcode* obtained via relative homological algebra is Lipschitz stable with respect to appropriate notions of distance [20, 88]. The computation of signed barcodes has been studied in several works, and is viable in some cases [19, 31, 42, 86]. However, for some proposed constructions of signed barcodes, size, computability, and instability are significant limitations [20, 70].

In the two-parameter case, signed barcodes provide a mathematically elegant way to fully visualize the rank invariant in a single 2-D plot [19]. However, even for very simple examples (e.g., interval modules whose support has a staircase shape), it can be challenging to interpret such a plot; in contrast, RIVET’s interactive visualization is straightforward to interpret, but does not fully visualize the rank invariant in a single plot. Apart from their use in visualization, signed barcodes have been used to construct features of data for machine learning [38, 84].

Multiparameter persistence modules with finite-dimensional vector spaces satisfy a Krull-Schmidt-Azumaya theorem, i.e., they decompose uniquely into indecomposable summands [17]. Recent work has introduced algorithms and software for computing such decompositions that is optimized for TDA input [54, 56]. Neither the definition of fibered barcode nor our scheme for fast queries of fibered barcodes depends on the decomposition of a multiparameter persistence module. However, when a decomposition of the input module M is available, this can potentially be exploited in the setting of our work, either to expedite the computation of the augmented arrangement (as proposed in [54]), or to provide more refined invariants. For the latter, some caution is warranted, as decompositions of multiparameter persistence modules are known to be unstable [7]. Recent work of Bjerkevik has introduced ideas for systematically handling this instability [10].

Data analysis using 2-parameter persistence, whether using the fibered barcode or other invariants, begins with the construction of a bifiltration from data. Following the initial

work of Carlsson and Zomorodian [28], which proposed several constructions of bifiltrations, many papers have introduced new bifiltrations of data and studied the theoretical and computational properties of bifiltrations, e.g., [2, 3, 4, 41, 51]. Much of this work has focused on density-sensitive bifiltrations of point cloud and metric data [1, 14, 15, 21, 46, 59, 60, 65, 77, 78, 79, 99], leading to substantial advances in our understanding of such bifiltrations, as well as new computational tools.

1.6 Outline

Section 2 covers preliminaries needed for the rest of the paper, including presentations, resolutions, Betti numbers, barcode computation, updates to RU -decompositions, and line arrangements. Section 3 defines the augmented arrangement $\mathcal{A}^\bullet(M)$ and proves Theorem 1.2 (i), which bounds the size of $\mathcal{A}^\bullet(M)$. Section 4 gives our algorithm for querying $\mathcal{A}^\bullet(M)$, establishes its correctness, and proves Theorem 1.3, which bounds the time complexity of a query. Section 5 gives our algorithm for computing $\mathcal{A}^\bullet(M)$ and Section 6 bounds its time and memory cost, thereby proving Theorem 1.2 (ii).

2 Mathematical Preliminaries

2.1 Free Persistence Modules and Presentations

Given a poset \mathbb{P} , a persistence module $M: \mathbb{P} \rightarrow \mathbf{Vec}$, an element $p \in \mathbb{P}$, and a vector $v \in M_p$, we write $\text{gr}(v) = p$. A *set of generators* for M is a set $G \subset \bigsqcup_{p \in \mathbb{P}} M_p$ such that for any $p \in \mathbb{P}$ and $v \in M_p$, we have

$$v = \sum_{i=1}^n c_i M_{\text{gr}(g_i), p}(g_i)$$

for some $g_1, \dots, g_n \in G$ and $c_1, \dots, c_n \in \mathbf{k}$.

For $p \in \mathbb{P}$, let $\mathbf{k}^{(p)}$ denote the persistence module given by

$$\mathbf{k}_q^{(p)} = \begin{cases} \mathbf{k} & \text{if } p \leq q, \\ 0 & \text{otherwise,} \end{cases} \quad \mathbf{k}_{q,r}^{(p)} = \begin{cases} \text{Id}_{\mathbf{k}} & \text{if } p \leq q, \\ 0 & \text{otherwise.} \end{cases}$$

We say a persistence module $F: \mathbb{P} \rightarrow \mathbf{Vec}$ is *free* if there exists a multiset \mathcal{G} of elements in \mathbb{P} such that $F \cong \bigoplus_{p \in \mathcal{G}} \mathbf{k}^{(p)}$. For F free, we define a *basis* of F to be a minimal set of generators for F . For B a basis of a finitely generated free module F , define $\beta^F: \mathbb{P} \rightarrow \mathbb{N}$ by

$$\beta^F(p) = |\{b \in B \mid \text{gr}(b) = p\}|.$$

Though bases of free modules are usually not unique, a straightforward linear algebra argument shows that β^F is independent of the choice of B .

A *morphism* of \mathbb{P} -indexed persistence modules $\eta: M \rightarrow N$ is a natural transformation, i.e., a collection of linear maps $\{\eta_p: M_p \rightarrow N_p\}_{p \in \mathbb{P}}$ such that $\eta_q \circ M_{p,q} = N_{p,q} \circ \eta_p$ for all $p \leq q \in \mathbb{P}$. With this definition of morphism, the persistence modules over a fixed poset form an abelian category, denoted $\mathbf{Vec}^{\mathbb{P}}$.

Given a morphism $\eta: F \rightarrow F'$ of finitely generated free \mathbb{P} -indexed persistence modules and ordered bases B and B' for F and F' , respectively, we represent η via a matrix $[\eta]$ with coefficients in the field \mathbf{k} , with each row and column labeled by an element of \mathbb{P} . To do so, note that η induces a map $\text{colim } \eta: \text{colim } F \rightarrow \text{colim } F'$, and B, B' induce bases for $\text{colim } F$ and $\text{colim } F'$, respectively. We take $[\eta]$ to be the usual matrix representation of $\text{colim } \eta$ with respect to these induced bases, with the i^{th} row given the label $\text{gr } B'_i$, and the j^{th} column given the label $\text{gr } B_j$. Regarding the morphism η as a functor $\{0 < 1\} \rightarrow \mathbf{Vec}^{\mathbb{P}}$, it is easily checked that $[\eta]$ determines η up to natural isomorphism.

A *presentation* of a persistence module $M: \mathbb{P} \rightarrow \mathbf{Vec}$ is a morphism $\eta: F \rightarrow F'$ of free persistence modules such that $M \cong \text{coker } \eta$, where $\text{coker } \eta := F'/\text{im } \eta$ is the cokernel of η . M is *finitely presented* if there exists a presentation $\eta: F \rightarrow F'$ of M with F and F' finitely generated. The above discussion makes clear that we can represent such η with respect to a choice of bases for F and F' as a matrix with \mathbb{P} -valued labels for the rows and columns; we call this labeled matrix a *presentation matrix* for M , or simply (abusing terminology slightly) a presentation.

We say a presentation $\eta: F \rightarrow F'$ of M is *minimal* if any presentation $\mu: E \rightarrow E'$ of M is naturally isomorphic to $\eta \oplus \nu$ for some ν of form

$$\nu: Y \oplus Z \xrightarrow{\text{Id}_Y \oplus 0} Y,$$

where Y and Z are free. By Azumaya's theorem [5], a minimal presentation is unique up to natural isomorphism. If $M: \mathbb{R}^d \rightarrow \mathbf{Vec}$ is a finitely presented persistence module, where \mathbb{R}^d is given the product partial order, then M has a minimal presentation $\eta: F \rightarrow F'$ with F and F' finitely generated; the analogous result for finitely generated \mathbb{Z} -graded $\mathbf{k}[x_1, x_2, \dots, x_d]$ -modules is proven in [91], and this proof adapts readily. We write $\beta_0^M = \beta^{F'}$ and $\beta_1^M = \beta^F$. More generally, one can define β_i^M for all $i \in \mathbb{N}$ in an analogous way using *minimal resolutions*. For $a \in \mathbb{R}^2$, $\beta_i^M(a)$ is called the i^{th} *Betti number* of M at a . By *Hilbert's syzygy theorem* [91], we have $\beta_i^M = 0$ for $i > d$.

2.2 Computation of Persistence Barcodes

We next discuss computation of the barcode $\mathcal{B}(M)$ of a persistence module M indexed by a finite totally ordered set, given as input a presentation matrix Q for M . We require that Q is *ordered*, meaning that the row and columns labels are both in increasing order. Typically, $\mathcal{B}(M)$ is computed by applying the *standard reduction* [57, 58, 109] to Q . This a variant of Gaussian elimination which performs left-to-right column additions to construct a certain factorization of Q , from which $\mathcal{B}(M)$ can be read off directly.

To elaborate, for any $m \times n$ matrix R , let R_{*j} denote the j^{th} column of R . If $R_{*j} \neq 0$, let ρ_j denote the maximum index of a non-zero entry in R_{*j} . We say R is *reduced* if $\rho_j \neq \rho_{j'}$ whenever $j \neq j'$ are the indices of non-zero columns in R . An *RU -decomposition* of an $r \times c$ matrix A is a matrix factorization $A = RU$ such that R is reduced and U is upper-triangular. The standard reduction computes an RU -decomposition of A in time $O(rc \cdot \min(r, c))$.

Given an RU -decomposition $Q = RU$ of our presentation matrix Q , we can read the barcode $\mathcal{B}(M)$ from R via the following result, where we denote the label of row i in Q as $\text{rl}(i)$ and the label of column j as $\text{cl}(j)$.

Proposition 2.1 ([44]). *For any RU -decomposition of Q , $\mathcal{B}(M)$ is determined from R as follows:*

$$\mathcal{B}(M) = \{[\text{rl}(\rho_j), \text{cl}(j)) \mid R_{*j} \neq 0\} \sqcup \{[\text{rl}(i), \infty) \mid R_{*i} = 0 \text{ and } i \neq \rho_j \text{ for any } j\}.$$

Although $\mathcal{B}(M)$ can be obtained from R , without considering U , maintaining U enables efficient updates to $\mathcal{B}(M)$ when the presentation matrix Q is modified [44], as we explain next.

2.3 Updating an RU -Decomposition

Motivated by the problem of computing the persistent homology of a parameterized family of data sets, Cohen-Steiner et al. [44] studied the problem of updating an RU -decomposition $Q = RU$ when the rows and columns of Q are permuted. We now briefly discuss the approach of [44], as well as closely related approaches to this problem appearing in subsequent work [22, 85, 92]. In Section 5.3, we apply RU -updates to compute barcode templates.

Given the RU -decomposition $Q = RU$ of an $r \times c$ matrix Q and permutation matrices P and P' of respective dimensions $r \times r$ and $c \times c$, the aim is to compute an RU -decomposition of $\hat{Q} := PQP'$ by updating R and U . Writing $\bar{R} := PRP'$ and $\bar{U} := (P')^{-1}UP'$, note that $\hat{Q} = \bar{R}\bar{U}$, but this is generally not an RU -decomposition of \hat{Q} , since \bar{R} might not be reduced and \bar{U} might not be upper triangular. We therefore perform matrix operations on \bar{R} and \bar{U} to obtain an RU -factorization $\hat{Q} = \hat{R}\hat{U}$. These updates can be done using the following *global strategy*, where we use the same notation for a matrix and the result after performing elementary operations on it:

1. Do downward row operations on \bar{U} to make it upper triangular, also doing the corresponding leftward column operations on \bar{R} .
2. Then do rightward column operations on \bar{R} to make it reduced, also doing the corresponding upward row operations on \bar{U} .

Note that the row operations performed in step 2 preserve the upper-triangular structure of \bar{U} . Hence, the resulting matrices \hat{R} and \hat{U} are reduced and upper triangular, respectively.

To see that $\hat{Q} = \hat{R}\hat{U}$, note that

$$\begin{aligned}\hat{R} &= \bar{R}A^{-1}B \\ \hat{U} &= B^{-1}A\bar{U},\end{aligned}$$

where left multiplication by A performs the row operations on \bar{U} in step 1, and right multiplication by B performs the column operations on $\bar{R}A^{-1}$ in step 2. Thus,

$$\hat{R}\hat{U} = (\bar{R}A^{-1}B)(B^{-1}A\bar{U}) = \bar{R}\bar{U} = \hat{Q},$$

as desired. This update scheme adapts readily to the setting where R and U^{-1} are maintained instead of R and U [22, 85, 92].

Step 1 can be done by ordinary Gaussian elimination, while step 2 can be done using the standard reduction mentioned in Section 2.2. However, if the permutations are known in advance to have special structure, then it may be advantageous to tailor the reduction algorithms to that structure. Cohen-Steiner et al. [44] considered the case where the permutations are transpositions of adjacent indices, and showed that a specialized version of the above update scheme, called a *vineyard update*, runs in time $O(r+c)$. This scheme can be extended to handle arbitrary permutations, simply by decomposing each permutation into a sequence of transpositions of adjacent rows or columns, and then applying a separate vineyard update for each transposition in the sequence. However, for general permutations, this can be quite expensive in practice, in part because quadratically many transpositions are required in the worst case. Thus, it can sometimes be more efficient in practice to perform a single global update to the RU -decomposition, as above, or to recompute the RU -decomposition from scratch. Luo and Nelson [85] consider such global updates in the setting where R and U^{-1} are maintained. As an alternative approach, Piekenbrock and Perea [92] introduce a variant of the vineyard update scheme that decomposes an arbitrary permutation into a sequence of *non-adjacent* transpositions. They then perform a separate update for each transposition in the sequence by applying an algorithm of Busaryev et al. [22].

Typically, the matrices arising in TDA applications are large and sparse, so they must be stored sparsely. To implement vineyard updates, [44] proposes to store R in a column-sparse way and U in a row-sparse way. With these choices, it is inexpensive to permute columns of R or rows of U , but it is expensive to permute rows of R or columns of U . Therefore, [44] permutes rows of R implicitly, by maintaining a separate array representation of the row permutation. Column permutations of U are handled analogously.

2.4 Line Arrangements

Line arrangements in (subregions of) \mathbb{R}^2 are classical objects in computational geometry. In this paper, we will only consider line arrangements in the right half plane $\mathcal{H} := [0, \infty) \times \mathbb{R}$.

Here, we define such arrangements and review standard results about computation, storage, and queries of line arrangements.

A *cell* is a topological space homeomorphic to \mathbb{R}^d for some $d \geq 0$. We define a *cell complex* on \mathcal{H} to be a decomposition of \mathcal{H} into finitely many cells, so that the topological boundary of each cell lies in the union of cells of lower dimension. In such a cell complex, some cells are unbounded, and each cell has dimension at most two.

A *line arrangement* in \mathcal{H} is the cell complex on \mathcal{H} induced by a finite set W of lines in \mathbb{R}^2 . For each $i \in \{0, 1, 2\}$, the maximum number of i -cells in such an arrangement is $\Theta(|W|^2)$ [101, Chapter 28]. We call the 0-cells, 1-cell, and 2-cells of the arrangement *vertices*, *edges*, and *faces*, respectively. The 1-skeleton of the arrangement (i.e., the union of vertices and edges) is

$$\partial\mathcal{H} \cup \left(\mathcal{H} \cap \bigcup_{\ell \in W} \ell \right).$$

The standard data structure for storing a line arrangement is the *doubly connected edge list (DCEL)*. This consists of a collection of vertices, edges, and faces, together with pointers specifying the facet relations. The size of the DCEL is proportional to the number of cells in the arrangement. The problem of computing a DCEL representation of a line arrangement, given the set of lines, has been extensively studied. The most popular algorithm for this, the *Bentley-Ottmann algorithm* [52], constructs the DCEL representation of a line arrangement with l lines and v vertices in time $O((l + v) \log l)$ and memory $O(l + v)$. There exist asymptotically faster algorithms for constructing line arrangements, e.g., an algorithm of Chazelle and Edelsbrunner [35] runs in time $O(l \log l + v)$. However, Bentley-Ottmann is a standard choice in software because it is simple and performs well in practice.

Point location, the problem of finding the cell in a line arrangement containing a given query point, is also well studied. As discussed in Section 1.3, our scheme for queries of fibered barcodes involves point location. To perform many point location queries or to perform queries in real time, one typically precomputes a data structure on which the queries can be performed efficiently. Let e denote the number of edges in the arrangement. There are several strategies which, in time $O(e \log e)$ and memory $O(e)$, compute a data structure on which we can perform a point location query in time $O(\log e)$; see [101, Chapter 38] and [52, Chapter 6]. In fact, these strategies apply to general polygonal subdivisions of the plane.

3 The Augmented Arrangement

In this section, we define $\mathcal{A}^\bullet(M)$, the *augmented arrangement* of a finitely presented bipersistence module M . First, in Section 3.1 we define the line arrangement $\mathcal{A}(M)$ underlying $\mathcal{A}^\bullet(M)$. In Section 3.2, we formally define the map push_ℓ from the plane onto an affine line ℓ of non-negative slope, first mentioned in Section 1.3. Using this, in Section 3.3 we define the barcode template \mathcal{B}^Δ stored at each face Δ of $\mathcal{A}^\bullet(M)$.

3.1 Definition of the Line Arrangement

Let \mathcal{L} denote the set of all affine lines in \mathbb{R}^2 . For $\mathcal{I} \subset \mathbb{R} \cup \{\infty\}$, we let $\mathcal{L}_{\mathcal{I}}$ denote the subset of \mathcal{L} consisting of lines whose slopes lie in \mathcal{I} . For example, $\mathcal{L}_{[0, \infty]}$ is the set of lines with non-negative, possibly infinite slope. Note that each $\ell \in \mathcal{L}_{[0, \infty]}$ is a totally ordered subset of \mathbb{R}^2 .

The following standard point-line duality gives a parameterization of $\mathcal{L}_{\mathbb{R}}$ by \mathbb{R}^2 :

$$\begin{aligned} (-)^*: \mathcal{L}_{\mathbb{R}} &\rightarrow \mathbb{R}^2 & (-)^*: \mathbb{R}^2 &\rightarrow \mathcal{L}_{\mathbb{R}} \\ y = qx + r &\mapsto (q, -r) & (q, r) &\mapsto y = qx - r. \end{aligned}$$

These maps are homeomorphisms with respect to the standard topology on \mathbb{R}^2 and the restriction to $\mathcal{L}_{\mathbb{R}}$ of the usual Grassmanian topology. It is easily checked that this duality preserves incidence, in the sense that for $a \in \mathbb{R}^2$ and $\ell \in \mathcal{L}_{\mathbb{R}}$, $a \in \ell$ if and only if $\ell^* \in a^*$; see Fig. 2. This point-line duality does not extend naturally to vertical lines.

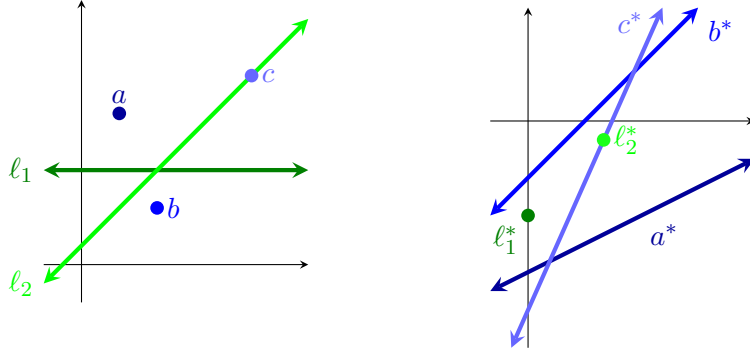


Figure 2: Illustration of point-line duality

Define $S \subset \mathbb{R}^2$ by $S = \text{supp } \beta_0^M \cup \text{supp } \beta_1^M$, where supp denotes the support. For X a finite subset of \mathbb{R}^2 , let $\vee X$ denote the *join of X* , i.e., the least upper bound of X in \mathbb{R}^2 . For example, $\vee\{(2, 0), (1, 1), (0, 2)\} = (2, 2)$. For $a, b \in \mathbb{R}^2$, we often write $\vee\{a, b\}$ as $a \vee b$.

Definition 3.1.

- (i) We call a pair of distinct elements $a, b \in \mathbb{R}^2$ *weakly incomparable* if either a and b are incomparable in the partial order on \mathbb{R}^2 , or a and b share a coordinate (i.e., $a_1 = b_1$ or $a_2 = b_2$).
- (ii) We call $\alpha \in \mathbb{R}^2$ an *anchor* if $\alpha = s \vee t$ for some weakly incomparable pair $s, t \in S$.

Definition 3.2. We define $\mathcal{A}(M)$ to be the line arrangement in \mathcal{H} induced by the set of lines

$$\{\alpha^* \mid \alpha \in \mathbb{R}^2 \text{ is an anchor}\}.$$

Remark 3.3. There are two types of vertices in the arrangement $\mathcal{A}(M)$: the intersection of the duals of two anchors, and the intersection of the dual of an anchor with $\partial\mathcal{H}$. These two types are not mutually exclusive, since the duals of two anchors with the same y -coordinate intersect on the line $\partial\mathcal{H}$. To better understand the first type of vertex, note that for two anchors $\alpha \neq \gamma$, α^* and γ^* intersect in \mathcal{H} if and only if there exists some $\ell \in \mathcal{L}_{[0,\infty)}$ containing both α and γ ; such ℓ exists precisely when α and γ are comparable and have distinct x -coordinates.

As in Section 1.4, let $\kappa = \kappa_x \kappa_y$, for κ_x and κ_y the number of unique x and y coordinates, respectively, of points in S . Clearly, the number of anchors is at most κ . Hence the number of lines in $\mathcal{A}(M)$, including $\partial\mathcal{H}$, is at most $\kappa + 1$. The size bounds mentioned in Section 2.4 thus imply that the numbers of vertices, edges, and faces in $\mathcal{A}(M)$ are each $\Theta(\kappa^2)$.

3.2 Push Maps

Recall that for each $\ell \in \mathcal{L}_{[0,\infty]}$, the partial order on \mathbb{R}^2 restricts to a total order on ℓ . This extends to a total order on $\ell \cup \{\infty\}$ by taking ∞ to be the maximum element.

Definition 3.4. For $\ell \in \mathcal{L}_{[0,\infty]}$, define the *push map* $\text{push}_\ell : \mathbb{R}^2 \rightarrow \ell \cup \{\infty\}$ by taking

$$\text{push}_\ell(a) = \min\{b \in \ell \mid a \leq b\},$$

where it is understood that the minimum over an empty set is ∞ .

Note that

- $\infty \in \text{im } \text{push}_\ell$ if and only if ℓ is either horizontal or vertical.
- For $a \in \mathbb{R}^2$ and $\text{push}_\ell(a) = c \in \ell$, either $a_1 = c_1$ or $a_2 = c_2$; see Fig. 3.
- push_ℓ preserves the partial order on \mathbb{R}^2 , i.e., $\text{push}_\ell(a) \leq \text{push}_\ell(b)$ for all $a \leq b \in \mathbb{R}^2$.

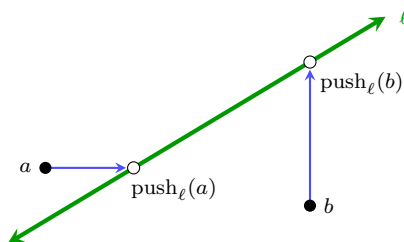


Figure 3: Illustration of push_ℓ for a line ℓ of positive, finite slope.

For any $a \in \mathbb{R}^2$, the maps $\{\text{push}_\ell\}_{\ell \in \mathcal{L}_{(0,\infty)}}$ induce a map

$$\text{push}_a : \mathcal{L}_{(0,\infty)} \rightarrow \mathbb{R}^2,$$

defined by $\text{push}_a(\ell) = \text{push}_\ell(a)$.

Lemma 3.5. For any $a \in \mathbb{R}^2$, the map push_a is continuous.

Proof. This follows from the observation that for any $\ell \in \mathcal{L}_{(0,\infty)}$, $\text{push}_a(\ell)$ is the unique intersection of ℓ with

$$\{(a_1, y) \mid y \geq a_2\} \cup \{(x, a_2) \mid x \geq a_1\}. \quad \square$$

For $\ell \in \mathcal{L}_{(0,\infty)}$, push_ℓ induces a totally ordered partition S^ℓ of S , where elements of the partition are level sets of the restriction of push_ℓ to S , and the total order on S^ℓ is the pullback of the total order on ℓ . We denote the i^{th} element of S^ℓ as S_i^ℓ . See Fig. 4 for an illustration.

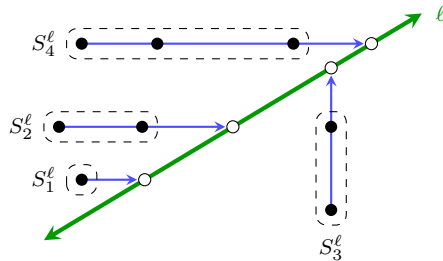


Figure 4: Illustration of a totally ordered partition S^ℓ of S . The elements of S are drawn as black dots.

The following result is the key to defining the augmented arrangement.

Theorem 3.6. If the duals of $\ell, \ell' \in \mathcal{L}_{(0,\infty)}$ are contained in the same (open) face of $\mathcal{A}(M)$, then $S^\ell = S^{\ell'}$.

Proof. Since point-line duality preserves incidence, the 1-skeleton of $\mathcal{A}(M)$ is

$$\{\ell^* \mid \ell \in \mathcal{L}_{(0,\infty)} \text{ contains an anchor}\} \cup \partial\mathcal{H}, \quad (3.1)$$

Moreover, $\partial\mathcal{H} = \{\ell^* \mid \ell \in \mathcal{L}_{\{0\}}\}$. Thus, since a face of $\mathcal{A}(M)$ is connected, it suffices to show that for any $\ell \in \mathcal{L}_{(0,\infty)}$ that contains no anchor, there is an open neighborhood $\mathcal{N} \subset \mathcal{L}_{(0,\infty)}$ of ℓ such that $S^\ell = S^{\ell'}$ for all $\ell' \in \mathcal{N}$. To show this, assume that $\ell \in \mathcal{L}_{(0,\infty)}$ contains no anchor, and consider distinct $s, t \in S$ with $\text{push}_\ell(s) = \text{push}_\ell(t)$. Note that s, t must lie either on the same horizontal line or the same vertical line; otherwise s and t would be incomparable and we would have $\text{push}_\ell(s) = \text{push}_\ell(t) = s \vee t \in \ell$, contradicting the assumption that ℓ contains no anchor. Assume without loss of generality that $s < t$ and s, t lie on the same horizontal line h . Then we must also have that $\text{push}_\ell(s) = \text{push}_\ell(t)$ lies on h . Since $t = s \vee t$, t is an anchor. However, ℓ does not contain any anchor, so we must have $t < \text{push}_\ell(t)$. Any sufficiently small perturbation ℓ' of ℓ will also intersect h at

a point a to the right of t , so that we have $\text{push}_{\ell'}(s) = \text{push}_{\ell'}(t) = a$. Thus for all ℓ' in a neighborhood of ℓ , $\text{push}_{\ell'}(s) = \text{push}_{\ell'}(t)$.

In fact, since S is finite, we can choose a single neighborhood \mathcal{N} of ℓ in $\mathcal{L}_{(0,\infty)}$ such that for any $s, t \in S$ with $\text{push}_\ell(s) = \text{push}_\ell(t)$, we have $\text{push}_{\ell'}(s) = \text{push}_{\ell'}(t)$ for all $\ell' \in \mathcal{N}$. In view of Lemma 3.5, by choosing \mathcal{N} to be smaller if necessary, we may also ensure that if $\text{push}_\ell(s) \neq \text{push}_\ell(t)$, then $\text{push}_{\ell'}(s) \neq \text{push}_{\ell'}(t)$ for all $\ell' \in \mathcal{N}$. Thus, the partition $S^{\ell'}$ is independent of the choice of $\ell' \in \mathcal{N}$. Finally, Lemma 3.5 also implies that the total order on $S^{\ell'}$ is independent of the choice of $\ell' \in \mathcal{N}$. \square

Remark 3.7. In fact, Theorem 3.6 can be strengthened to show that for any $\ell, \ell' \in \mathcal{L}_{(0,\infty)}$, the duals of ℓ and ℓ' lie in the same cell of $\mathcal{A}(M)$ if and only if $S^\ell = S^{\ell'}$. However, we will not need the full generality of this stronger result.

To derive our main algorithm for computing the augmented arrangement, in Section 5.2 we give a detailed analysis of the relationship between S^ℓ and $S^{\ell'}$ for lines ℓ and ℓ' lying in neighboring faces of $\mathcal{A}(M)$. A simple such case is illustrated in Fig. 5; see also Fig. 10 for further examples.

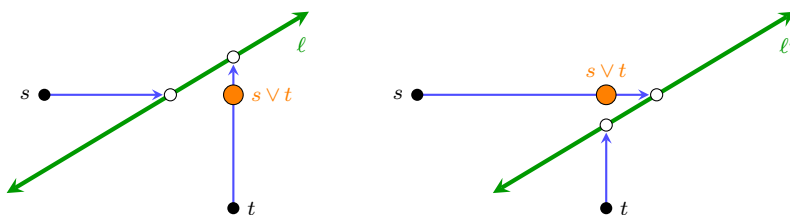


Figure 5: An illustration of how incomparable points $s, t \in S$ push onto lines ℓ and ℓ' lying above and below the anchor $s \vee t$. The dual points ℓ^* and ℓ'^* lie in neighboring 2-cells of $\mathcal{A}(M)$ with shared boundary lying on $(s \vee t)^*$. Note that $\text{push}_\ell(s) < \text{push}_\ell(t)$ and $\text{push}_{\ell'}(t) < \text{push}_{\ell'}(s)$, i.e., the order in which the points push onto the line switches as the line changes.

3.3 Barcode Templates

Fixing a face Δ of $\mathcal{A}(M)$, we now define the barcode template \mathcal{B}^Δ stored at the face Δ in the augmented arrangement $\mathcal{A}^\bullet(M)$.

Definition 3.8. Theorem 3.6 yields a totally ordered partition

$$S^\Delta = \{S_1^\Delta, \dots, S_k^\Delta\}$$

of S , given by $S^\Delta = S^\ell$ for any line ℓ with $\ell^* \in \Delta$. For each S_i^Δ , we let

$$\mathcal{P}_i^\Delta = \bigvee \left(\bigcup_{j \leq i} S_j^\Delta \right).$$

The set of *template points* at Δ is $\{\mathcal{P}_1^\Delta, \dots, \mathcal{P}_k^\Delta\}$.

In words, elements of \mathcal{P}^Δ are joins of unions of prefixes of S^Δ . See Fig. 6 for an illustration. Note that \mathcal{P}^Δ is a subset of \mathbb{R}^2 and that, by construction, the restriction of the partial order on \mathbb{R}^2 to \mathcal{P}^Δ is a total order. We let M^Δ denote the restriction of M to \mathcal{P}^Δ . Since M is assumed to be finitely presented, M^Δ is p.f.d., so it has a well-defined barcode $\mathcal{B}(M^\Delta)$.

Definition 3.9. We call $\mathcal{B}^\Delta := \mathcal{B}(M^\Delta)$ the *barcode template* at Δ .

$\mathcal{B}(M^\Delta)$ consists of intervals $[a, b) \subset \mathcal{P}^\Delta$ with $a < b \in \mathcal{P}^\Delta \cup \{\infty\}$. Identifying each interval $[a, b)$ with the pair (a, b) , we recover the form of the barcode template specified in Section 1.3.

Definition 3.10. The *augmented arrangement* $\mathcal{A}^\bullet(M)$ consists of the line arrangement $\mathcal{A}(M)$ and a data structure for log-time point location queries in $\mathcal{A}(M)$ as in Section 2.4, together with the barcode templates \mathcal{B}^Δ at all faces Δ of $\mathcal{A}(M)$.

Remark 3.11. The fibered barcode $\mathcal{F}(M)$ determines neither the Betti numbers of M nor the resulting set of anchors; see [79, Example 2.2]. Hence $\mathcal{F}(M)$ does not determine $\mathcal{A}^\bullet(M)$. We expect that by defining the set of anchors differently, one can obtain a variant of $\mathcal{A}^\bullet(M)$ which depends only on $\mathcal{F}(M)$. We leave the exploration of this to future work.

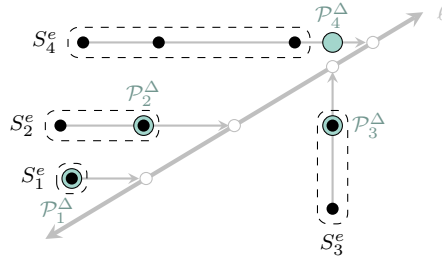


Figure 6: Illustration of template points \mathcal{P}^Δ (light blue), for S and ℓ as in Fig. 4 and Δ the face containing ℓ^* .

Having defined the augmented arrangement, it is now easy to see that it satisfies the size bound of Theorem 1.2 (i):

Proof of Theorem 1.2 (i). As noted in Section 3.1, $\mathcal{A}(M)$ has size $O(\kappa^2)$. The point location data structure has size linear in the number of edges in $\mathcal{A}(M)$, so also has size $O(\kappa^2)$. Since $\mathcal{A}^\bullet(M)$ stores a barcode template of size $O(m)$ for each face of $\mathcal{A}(M)$, the total size of all barcode templates is $O(m\kappa^2)$. Thus, the total size of $\mathcal{A}^\bullet(M)$ is $O(m\kappa^2)$. \square

4 Querying the Augmented Arrangement

We now specify the procedure to query $\mathcal{A}^\bullet(M)$ for the barcode $\mathcal{B}(M^\ell)$ of a given line $\ell \in \mathcal{L}_{[0,\infty]}$. The main result of this section, Theorem 4.2, establishes the correctness of this procedure. In Section 4.3, we discuss the computational details of our queries and bound the complexity of a query, proving Theorem 1.3.

4.1 The Query Procedure

The query of $\mathcal{A}^\bullet(M)$ for the barcode $\mathcal{B}(M^\ell)$ involves two main steps. First, we choose a face Δ in $\mathcal{A}(M)$, as specified below. Second, we obtain the intervals of $\mathcal{B}(M^\ell)$ from the pairs of \mathcal{B}^Δ by pushing the points in each pair $(a, b) \in \mathcal{B}^\Delta$ onto the line ℓ , via the map push_ℓ of Section 3.2.

If ℓ is not vertical, then we choose Δ to be a 2-dimensional coface of ℓ^* (meaning that ℓ^* is in the closure of Δ); if ℓ contains no anchor, then there is only one such coface. In more detail, we choose Δ as follows (see Fig. 7 for an illustration):

- If ℓ is neither horizontal nor vertical, then we choose Δ to be any 2-D coface of ℓ^* .
- If ℓ is horizontal, say ℓ is the line $y = c$, then we take Δ to be the face whose points are dual to lines ℓ' of positive slope lying above all anchors with y -coordinate at most c and lying below all anchors with y -coordinate greater than c . (It is helpful to think of the line ℓ' as arising as a certain small perturbation of ℓ , as in Fig. 7.)
- Symmetrically, if ℓ is vertical, say ℓ is the line $x = c$, then we take Δ to be the face whose points are dual to lines ℓ' of positive slope lying right of all anchors with x -coordinate at most c and lying left of all anchors with x -coordinate greater than c .

Remark 4.1. For ℓ horizontal or vertical, the face Δ can be described directly in terms of $\mathcal{A}(M)$, as follows: If ℓ is the horizontal line $y = c$, then since ℓ has slope 0, $\ell^* \in \partial\mathcal{H}$. If ℓ^* is contained in an edge of $\mathcal{A}(M)$, then Δ is the unique coface of this edge. Otherwise, ℓ^* is a vertex of $\mathcal{A}(M)$. Then the 2-D cofaces of ℓ^* are ordered vertically in \mathcal{H} and Δ is the bottom such coface.

If ℓ is the vertical line $x = c$, let k be the line in the arrangement $\mathcal{A}(M)$ of maximum slope, among those having slope at most c , if a unique such line exists; if there are several such lines, then take k to be the one with the largest y -intercept. Then k contains a unique unbounded edge in $\mathcal{A}(M)$ and Δ is the face lying directly above this edge. (To see why this choice of Δ is correct, note that points in Δ are dual to lines of large slope which lie

below k^* .) If a line k as above does not exist, then Δ is the bottom unbounded face of $\mathcal{A}(M)$; since $\mathcal{A}(M)$ contains no vertical lines besides $\partial\mathcal{H}$, this face is uniquely defined.

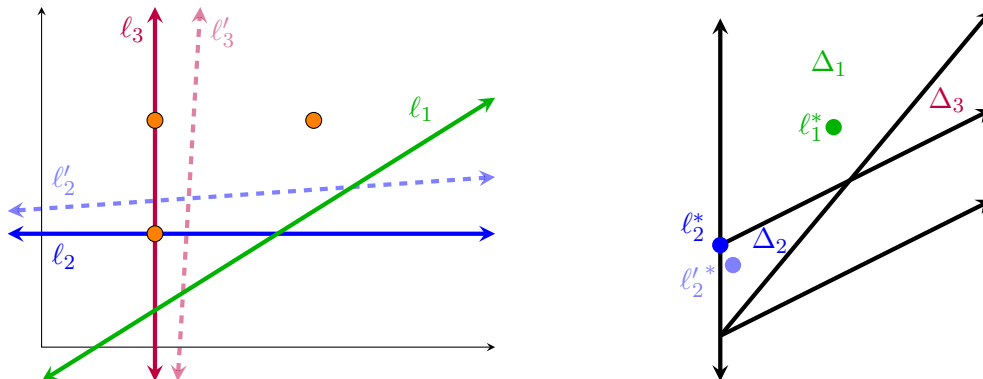


Figure 7: Three anchors are drawn at left in orange; the corresponding line arrangement $\mathcal{A}(M)$ is shown at right. For each line ℓ_i at left, the corresponding face Δ_i , chosen as in Section 4.1, is labeled at right in the same color. For the horizontal line ℓ_2 and vertical line ℓ_3 , choices of the perturbations ℓ'_2 and ℓ'_3 are also shown at left as dashed lines. The duals ℓ_1^* , ℓ_2^* , and $\ell_2'^*$ are also shown at right. The dual point $\ell_3'^*$ is not shown because this point has very large coordinates, since ℓ'_3 is nearly vertical.

4.2 Correctness of the Query Procedure

Theorem 4.2. *For any line $\ell \in \mathcal{L}_{[0,\infty]}$ and a face Δ chosen as above, we have*

$$\mathcal{B}(M^\ell) = \{ [\text{push}_\ell(a), \text{push}_\ell(b)] \mid [a, b] \in \mathcal{B}^\Delta, \text{push}_\ell(a) < \text{push}_\ell(b) \},$$

where we take $\text{push}_\ell(\infty) = \infty$.

Note that if ℓ^* lies in a face of $\mathcal{A}(M)$, then that face is necessarily Δ , and we have $\text{push}_\ell(a) < \text{push}_\ell(b)$ for all $(a, b) \in \mathcal{B}^\Delta$. Thus, the theorem statement simplifies for such ℓ . However, if ℓ^* is contained in the 1-skeleton of $\mathcal{A}(M)$, then it is possible to have $\text{push}_\ell(a) = \text{push}_\ell(b)$.

We prepare for the proof of Theorem 4.2 with three lemmas. For $a \in \mathbb{R}^2$, let

$$R(a) = \{s \in S \mid s \leq a\}.$$

Lemma 4.3. *For $a \leq b \in \mathbb{R}^2$ with $R(a) = R(b)$, $M_{a,b}$ is an isomorphism.*

Proof. Let $\eta : F \rightarrow F'$ be a minimal presentation for M . It is easy to check that $F_{a,b}$ and $F'_{a,b}$ are both isomorphisms. As we have

$$F'_{a,b} \circ \eta_a = \eta_b \circ F_{a,b},$$

$F'_{a,b}$ descends to an isomorphism on $\text{coker}(\eta) \cong M$. □

Given totally ordered sets \mathbb{T} and \mathbb{U} with \mathbb{T} finite, a functor (i.e., order-preserving function) $\mathcal{E} : \mathbb{T} \rightarrow \mathbb{U}$, and a functor $N : \mathbb{T} \rightarrow \mathbf{Vec}$, we let $\text{Lan}_{\mathcal{E}}(N) : \mathbb{U} \rightarrow \mathbf{Vec}$ denote the left Kan extension of N along \mathcal{E} [95, Section 6.1]. Then $\text{Lan}_{\mathcal{E}}(N)$ admits the following simple, elementary description: For $u \in \mathbb{U}$, let

$$\mathcal{E}_{\leq u} = \{t \in \mathbb{T} \mid \mathcal{E}(t) \leq u\}.$$

If $\mathcal{E}_{\leq u} \neq \emptyset$ we define

$$\mathcal{E}^{-1}(u) = \max \mathcal{E}_{\leq u},$$

Then $\text{Lan}_{\mathcal{E}}(N) : \mathbb{U} \rightarrow \mathbf{Vec}$ is given by

$$\begin{aligned} \text{Lan}_{\mathcal{E}}(N)_u &= \begin{cases} N_{\mathcal{E}^{-1}(u)} & \text{if } \mathcal{E}_{\leq u} \neq \emptyset, \\ 0 & \text{otherwise.} \end{cases} \\ \text{Lan}_{\mathcal{E}}(N)_{u,v} &= \begin{cases} N_{\mathcal{E}^{-1}(u), \mathcal{E}^{-1}(v)} & \text{if } \mathcal{E}_{\leq u} \neq \emptyset \\ 0 & \text{otherwise.} \end{cases} \end{aligned}$$

Lemma 4.4. *Given totally ordered sets \mathbb{T} and \mathbb{U} with \mathbb{T} finite, a functor $\mathcal{E} : \mathbb{T} \rightarrow \mathbb{U}$, and a p.f.d. functor $N : \mathbb{T} \rightarrow \mathbf{Vec}$,*

$$\mathcal{B}(\text{Lan}_{\mathcal{E}}(N)) = \{[\mathcal{E}(s), \mathcal{E}(t)] \mid [s, t] \in \mathcal{B}(N), \mathcal{E}(s) < \mathcal{E}(t)\},$$

where we define $\mathcal{E}(\infty) = \infty$.

Proof. It is easy to check directly that the map $N \mapsto \text{Lan}_{\mathcal{E}}(N)$ preserves direct sums. (More generally, left Kan extensions preserve coproducts, because they are left adjoints [95, Proposition 6.1.5], and left adjoints preserve colimits [95, Theorem 4.5.3].) Hence, it suffices to prove the result in the case that the barcode of N contains a single interval. In this case, it is easy to check the result directly from the concrete description of $\text{Lan}_{\mathcal{E}}(N)$ given above. □

Lemma 4.5. *Given a line $\ell \in \mathcal{L}_{(0, \infty)}$ and $a^1, \dots, a^n \in \mathbb{R}^2$, we have*

$$\text{push}_{\ell}(\vee\{a^1, \dots, a^n\}) = \max(\text{push}_{\ell}(a^i)).$$

Proof. Let $b = \vee \{a^1, \dots, a^n\}$. We prove the result assuming that b is either on or below ℓ ; if b is above ℓ , a symmetric argument applies. Given the assumption, b and $\text{push}_\ell(b)$ have the same x -coordinate, which is also the x -coordinate of some a^j . Since $a^j \leq b$, a^j also lies on or below ℓ , so we have $\text{push}_\ell(a^j) = \text{push}_\ell(b)$. Therefore, $\max(\text{push}_\ell(a^i)) \geq \text{push}_\ell(b)$. But since each $a^i \leq b$ and push_ℓ respects the partial order in \mathbb{R}^2 , the reverse inequality $\max(\text{push}_\ell(a^i)) \leq \text{push}_\ell(b)$ also holds. \square

Proof of Theorem 4.2. Let $\mathcal{Q} = \mathcal{P}^\Delta \cap (\text{push}_\ell)^{-1}(\ell)$, i.e., \mathcal{Q} is the subset of \mathcal{P}^Δ which pushes onto ℓ , rather than onto ∞ . Note that $\mathcal{Q} = \mathcal{P}^\Delta$ unless ℓ is horizontal or vertical. Let $\mathcal{E}: \mathcal{Q} \rightarrow \ell$ denote the restriction of push_ℓ to \mathcal{Q} . Note that \mathcal{E} is a functor between totally ordered sets. Let N denote the restriction of M^Δ (hence of M) to \mathcal{Q} . Then $\mathcal{B}(N)$ is given as follows:

$$\mathcal{B}(N) = \{[a, b] \in \mathcal{B}^\Delta \mid a, b \in \mathcal{Q} \cup \{\infty\}\} \cup \{[a, \infty) \mid [a, b] \in \mathcal{B}^\Delta, a \in \mathcal{Q}, b \in \mathcal{P}^\Delta \setminus \mathcal{Q}\}.$$

Lemma 4.4 then implies that

$$\mathcal{B}(\text{Lan}_\mathcal{E}(N)) = \{[\text{push}_\ell(a), \text{push}_\ell(b)] \mid [a, b] \in \mathcal{B}^\Delta, \text{push}_\ell(a) < \text{push}_\ell(b)\}.$$

Thus, to prove the result, it suffices to show that $\text{Lan}_\mathcal{E}(N) \cong M^\ell$. Note that for all $a \in \ell$,

$$\text{Lan}_\mathcal{E}(N)_a = \begin{cases} M_{\mathcal{E}^{-1}(a)} & \text{if } \mathcal{E}_{\leq a} \neq \emptyset, \\ 0 & \text{otherwise,} \end{cases}$$

where we have used the fact that $N_{\mathcal{E}^{-1}(a)} = M_{\mathcal{E}^{-1}(a)}$.

We now define a natural transformation $f: \text{Lan}_\mathcal{E}(N) \rightarrow M^\ell$ by

$$f_a = \begin{cases} M_{\mathcal{E}^{-1}(a), a} & \text{if } \mathcal{E}_{\leq a} \neq \emptyset, \\ 0 & \text{otherwise.} \end{cases}$$

Because the internal maps of both $\text{Lan}_\mathcal{E}(N)$ and M^ℓ are given in terms of the structure maps of M , f is indeed a natural transformation. We now show that f is a natural isomorphism. Note that if $\mathcal{E}_{\leq a} = \emptyset$, then $M_a = 0$. Hence, f_a is an isomorphism, because then its domain and codomain are both trivial.

It remains to check that if $\mathcal{E}_{\leq a} \neq \emptyset$, then $f_a = M_{\mathcal{E}^{-1}(a), a}$ is an isomorphism. By Lemma 4.3, it suffices to show that

$$R(\mathcal{E}^{-1}(a)) = R(a).$$

Since $\mathcal{E}^{-1}(a) \leq a$, we have $R(\mathcal{E}^{-1}(a)) \subset R(a)$. To show that $R(a) \subset R(\mathcal{E}^{-1}(a))$, consider $s \in R(a)$. We need to show that $s \leq \mathcal{E}^{-1}(a)$. By definition, we have

$$\mathcal{E}^{-1}(a) = \max \{\mathcal{P}_j^\Delta \in \mathcal{P}^\Delta \mid \text{push}_\ell(\mathcal{P}_j^\Delta) \leq a\}. \quad (4.1)$$

Let us write $\mathcal{E}^{-1}(a) = \mathcal{P}_i^\Delta$. First, consider the case that ℓ is neither horizontal or vertical. If $s \not\leq \mathcal{P}_i^\Delta$, then $s \in S_j^\Delta$ for some $j > i$. Suppose $s \in S_{j'}^\ell$. Since ℓ^* is in the closure of Δ , Lemma 3.5 implies that if $t \in S_k^\Delta$ for some $k \leq j$, then $t \in S_{k'}^\ell$ for some $k' \leq j'$. Therefore,

$$\bigcup_{k=1}^j S_k^\Delta \subset \bigcup_{k=1}^{j'} S_k^\ell. \quad (4.2)$$

Since $s \leq a$ and $a \in \ell$, we have $\text{push}_\ell(s) \leq a$. Then $\text{push}_\ell(t) \leq a$ for all $t \in S_k^\ell$ with $k \leq j'$. Hence, by Eq. (4.2), we have that $\text{push}_\ell(t) \leq a$ for all $t \in S_k^\Delta$ with $k \leq j$. Lemma 4.5 now implies that $\text{push}_\ell(\mathcal{P}_j^\Delta) \leq a$, contradicting the definition of $\mathcal{E}^{-1}(a)$ as a maximum, as in Eq. (4.1).

To finish the proof, we consider the case that ℓ is horizontal, say ℓ is the line $y = c$; the argument for vertical lines is symmetric. By the way we have chosen Δ , S^Δ consists of sets

$$V_x := \{s \in S \mid s_1 = x \text{ and } s_2 \leq c\},$$

as well as sets

$$H_y := \{s \in S \mid s_2 = y\}$$

for $y > c$, with the sets V_x ordered with respect to x and each V_x ordered before each H_y ; see Fig. 8 for an illustration. It follows that for $a = (a_1, c) \in \ell$, we have

$$\mathcal{E}^{-1}(a) = \bigvee \left(\bigcup_{x \leq a_1} V_x \right) = \bigvee \{s \in S \mid s \leq a\},$$

and therefore

$$R(\mathcal{E}^{-1}(a)) = \{s \in S \mid s \leq a\} = R(a). \quad \square$$

4.3 Computational Details and Complexity of Queries

We now discuss the computational details of our queries and bound the complexity of a query. We assume that the augmented arrangement $\mathcal{A}^\bullet(M)$ has already been computed as described in Section 5 below. Given a line $\ell \in \mathcal{L}_{[0, \infty]}$, the query of $\mathcal{A}^\bullet(M)$ for $\mathcal{B}(M^\ell)$ proceeds in two steps. The first step performs a search for the face Δ of $\mathcal{A}(M)$ specified in Section 4.1. Once the face Δ is selected, we obtain $\mathcal{B}(M^\ell)$ from \mathcal{B}^Δ by applying push_ℓ to the endpoints of each pair $(a, b) \in \mathcal{B}^\Delta$.

The search for face Δ works as follows: If $\ell \in \mathcal{L}_{[0, \infty]}$ (i.e., ℓ is not vertical), then it suffices to find the cell of $\mathcal{A}(M)$ containing ℓ^* . To do so, we use the point location data structure for $\mathcal{A}(M)$ that is part of $\mathcal{A}^\bullet(M)$; see Definition 3.10. Since $\mathcal{A}(M)$ has $O(\kappa^2)$ vertices, the search data structure has size $O(\kappa^2)$, and each point location query takes time $O(\log \kappa)$.

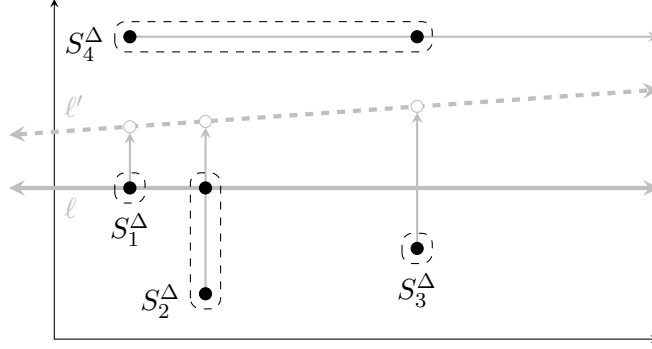


Figure 8: The sets $S_i^\Delta = S_i^{\ell'}$, for a horizontal line ℓ and Δ the face containing the dual of the perturbed line ℓ' , as specified in Section 4.1. The figure illustrates that the sets S_i^Δ are of the form V_x or H_y specified in the proof of Theorem 4.2.

If ℓ is vertical, then ℓ^* is not defined, and we require a different approach to find the face Δ . We precompute a separate, simpler search data structure to handle the case of vertical lines: Let \mathcal{K} denote the set of lines k in $\mathcal{A}(M)$ such that there is no other line in $\mathcal{A}(M)$ with the same slope lying above k . We take \mathcal{K} to be ordered by slope, and denote the i^{th} element of \mathcal{K} as \mathcal{K}_i . We compute a 1-D array whose i^{th} entry is a pointer to the rightmost (unbounded) edge of $\mathcal{A}(M)$ contained in \mathcal{K}_i . Given $\mathcal{A}(M)$, computing this array takes $O(n)$ time, where $n = O(\kappa)$ is the number of anchor lines. It follows from the description of the face Δ given in Remark 4.1 that for any vertical line ℓ , we can find Δ in $O(\log n)$ time by a binary search of this array.

We are now ready to prove Theorem 1.3, which bounds the cost of querying $\mathcal{A}^\bullet(M)$ for a barcode $\mathcal{B}(M^\ell)$.

Proof of Theorem 1.3. From the discussion above, it is clear that once we have precomputed the appropriate data structures, finding the face Δ takes $O(\log \kappa)$ time. Each evaluation of push_ℓ takes constant time, so computing $\mathcal{B}(M^\ell)$ from \mathcal{B}^Δ takes total time $O(|\mathcal{B}^\Delta|)$. Thus, the total time to query $\mathcal{A}^\bullet(M)$ for $\mathcal{B}(M^\ell)$ is $O(|\mathcal{B}^\Delta| + \log \kappa)$. If $\ell^* \in \Delta$, then $|\mathcal{B}^\Delta| = |\mathcal{B}(M^\ell)|$; this gives Theorem 1.3 (i). If $\ell^* \notin \Delta$, it may not be that $|\mathcal{B}^\Delta| = |\mathcal{B}(M^\ell)|$, but we do have $|\mathcal{B}^\Delta| = |\mathcal{B}(M^{\ell'})|$ for ℓ' an arbitrarily small perturbation of ℓ with $\ell'^* \in \Delta$. Theorem 1.3 (ii) follows. \square

5 Computing the Augmented Arrangement

Our algorithm for computing the augmented arrangement $\mathcal{A}^\bullet(M)$ takes as input a minimal presentation of M . The algorithm computes each of the following:

1. the set of anchors of M ,

2. the line arrangement $\mathcal{A}(M)$ and data structure for point location in $\mathcal{A}(M)$,
3. the barcode templates \mathcal{B}^Δ at all faces Δ .

Recall that the row and column labels of a minimal presentation for M encode the 0th and 1st Betti numbers of M , respectively, and hence immediately yield S , the union of the support of these Betti numbers. Given S , we can readily compute the set of anchors of M in $O(\kappa)$ time and $O(\kappa)$ memory by iterating through the minimal grid containing S in lexicographical order; we omit the easy details. Since the anchors of M correspond under point-line duality to the lines other than $\partial\mathcal{H}$ in $\mathcal{A}(M)$, once the anchors have been computed we can use the standard algorithms mentioned in Section 2.4 to compute $\mathcal{A}(M)$ and a point location data structure for $\mathcal{A}(M)$.

5.1 Computing the Barcode Templates

In the remainder of this section, we explain the computation of the barcode templates. For each face Δ of $\mathcal{A}(M)$, we define the surjective map

$$\text{lift}^\Delta : S \rightarrow \mathcal{P}^\Delta$$

where $\text{lift}^\Delta(s) = \mathcal{P}_i^\Delta$ for all $s \in S_i^\Delta$. Given a presentation matrix Q for M , we can obtain an ordered presentation matrix Q^Δ for M^Δ by applying lift^Δ to every row and column label of Q and then permuting the rows and columns of Q so that both the row and column labels are in increasing order. (Here and throughout, our convention is that a permutation of the rows or columns of a labeled matrix also permutes the labels.) We call such Q^Δ an *induced presentation* of M^Δ . We let σ_Δ and τ_Δ denote the respective choices of row and column permutations used to form Q^Δ .

By Proposition 2.1, the barcode template \mathcal{B}^Δ can be read from an RU -decomposition of Q^Δ . Naïvely, we could compute Q^Δ and its RU -decomposition from scratch at each face Δ , but this is inefficient. Instead, our algorithm updates the RU -decomposition at one face to obtain the RU -decomposition at a neighboring face.

To elaborate, let G denote the *dual graph* of $\mathcal{A}(M)$, i.e., the undirected graph with vertices the faces of $\mathcal{A}(M)$ and edges the pairs of adjacent faces; see Fig. 9 for an illustration. Let Δ_0 be the topmost face in $\mathcal{A}(M)$; Δ_0 contains the dual of each line to the right of all points in S . We compute a walk

$$\Gamma = \Delta_0, \Delta_1, \dots, \Delta_n$$

in G that visits each face at least once, as explained in Section 5.5 below.

For each i , we compute an RU -decomposition $Q^{\Delta_i} = R^{\Delta_i}U^{\Delta_i}$ of an induced presentation Q^{Δ_i} for M^{Δ_i} . For $i < n$, we compute the RU -decomposition of $Q^{\Delta_{i+1}}$ by updating the RU -decomposition of Q^{Δ_i} . To enable efficient RU -updates, we will require not only that each Q^{Δ_i} be an ordered presentation, but that it be *strongly ordered*, in the following sense:

Definition 5.1. We say that Q^{Δ_i} is strongly ordered if

- It is an ordered presentation (see Section 2.2),
- Given rows j and k of Q with (S -valued) labels s and t such that $\text{lift}^{\Delta_i}(s) = \text{lift}^{\Delta_i}(t)$ and $s < t$ in the partial order on \mathbb{R}^2 , we have $\sigma_{\Delta_i}(j) < \sigma_{\Delta_i}(k)$; and similarly for columns.

We compute Q^{Δ_0} and its RU -decomposition as follows: Since Δ_0 contains the duals of all lines lying to the right of S , we have that for all $s \in S$,

$$\text{lift}^{\Delta_0}(s) = (\max\{t_1 \mid t \in S, t_2 \leq s_2\}, s_2).$$

Therefore, to compute $\mathcal{P}^{\Delta_0} = \text{im lift}^{\Delta_0}$ and lift^{Δ_0} , it suffices to sort S in colexicographical order (i.e., where s is ordered before t if and only if $s_2 < t_2$ or $s_2 = t_2$ and $s_1 < t_1$), and then traverse S in increasing order. Computing Q^{Δ_0} amounts to sorting the rows and columns of Q with respect to the colexicographical order on labels, and then applying lift^{Δ_0} to each label. We can then compute an RU -decomposition of Q^{Δ_0} via the standard reduction mentioned in Section 2.2.

For $0 \leq i < n$, write $\Delta = \Delta_i$ and $\hat{\Delta} = \Delta_{i+1}$. Suppose we have computed the RU -decomposition $Q^\Delta = R^\Delta U^\Delta$. We compute an RU -decomposition of $Q^{\hat{\Delta}}$ for $M^{\hat{\Delta}}$, in three steps:

1. update \mathcal{P}^Δ and lift^Δ to obtain $\mathcal{P}^{\hat{\Delta}}$ and $\text{lift}^{\hat{\Delta}}$,
2. permute the rows and columns of R^Δ and U^Δ to obtain a matrix decomposition $Q^{\hat{\Delta}} = \bar{R}\bar{U}$ (which is not necessarily an RU -decomposition),
3. reduce the matrices \bar{R} and \bar{U} obtain an RU -decomposition of $Q^{\hat{\Delta}}$.

The next three subsections discuss these steps in detail.

5.2 Updating the Template Points and Lift Map

To explain how the template points and lift map change when passing from face Δ to the adjacent face $\hat{\Delta}$, suppose that the line containing the shared boundary of faces Δ and $\hat{\Delta}$ is dual to anchor α . Then α is an element of both \mathcal{P}^Δ and $\mathcal{P}^{\hat{\Delta}}$, as illustrated in Fig. 10. Suppose that $\alpha = \mathcal{P}_j^\Delta$. We distinguish between three cases, which are illustrated in Fig. 10.

Generic case: $\alpha = \vee(s, t)$ for some incomparable $s, t \in S$.

Merge case: $S_j^\Delta = \{\alpha\}$. In this case, S_{j-1}^Δ and S_j^Δ merge to form $S_{j-1}^{\hat{\Delta}}$; see Lemma 5.2 (ii) below.

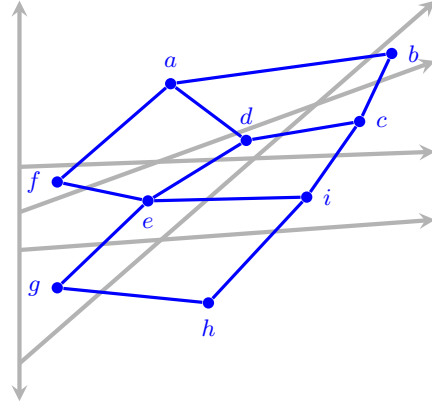


Figure 9: A line arrangement $\mathcal{A}(M)$ (in gray), together with its dual graph G (in blue). The walk Γ through G might visit the vertices in the order $a, b, c, d, e, f, e, g, h, i$.

Split case: $S_{j+1}^{\hat{\Delta}} = \{\alpha\}$. In this case S_j^{Δ} splits into $S_j^{\hat{\Delta}}$ and $S_{j+1}^{\hat{\Delta}}$; see Lemma 5.2 (iii) below.

It is easily checked that these cases are mutually exclusive and cover all possible cases. If S is generic in the sense that no two elements of S share a coordinate, then only the first case arises, which explains our choice of name for this case. The merge case and split cases are symmetric, in the sense that if passing from Δ to $\hat{\Delta}$ is a merge, then passing from $\hat{\Delta}$ to Δ is a split, and vice versa; see Figs. 10 (b) and 10 (c).

The following result relates the totally ordered partitions S^{Δ} and $S^{\hat{\Delta}}$. We omit the easy proof.

Lemma 5.2.

(i) In the generic case, we have $|S^{\hat{\Delta}}| = |S^{\Delta}|$ and

$$S_i^{\hat{\Delta}} = \begin{cases} S_i^{\Delta} & \text{if } i \notin \{j-1, j\}, \\ S_j^{\Delta} \setminus \{\alpha\} & \text{if } i = j-1, \\ S_{j-1}^{\Delta} \cup \{\alpha\} & \text{if } i = j \text{ and } \alpha \in S, \\ S_{j-1}^{\Delta} & \text{if } i = j \text{ and } \alpha \notin S. \end{cases}$$

(ii) In the merge case, we have $|S^{\hat{\Delta}}| = |S^{\Delta}| - 1$ and

$$S_i^{\hat{\Delta}} = \begin{cases} S_i^{\Delta} & \text{if } i < j-1, \\ S_{j-1}^{\Delta} \cup \{\alpha\} & \text{if } i = j-1, \\ S_{i+1}^{\Delta} & \text{if } i > j-1. \end{cases}$$

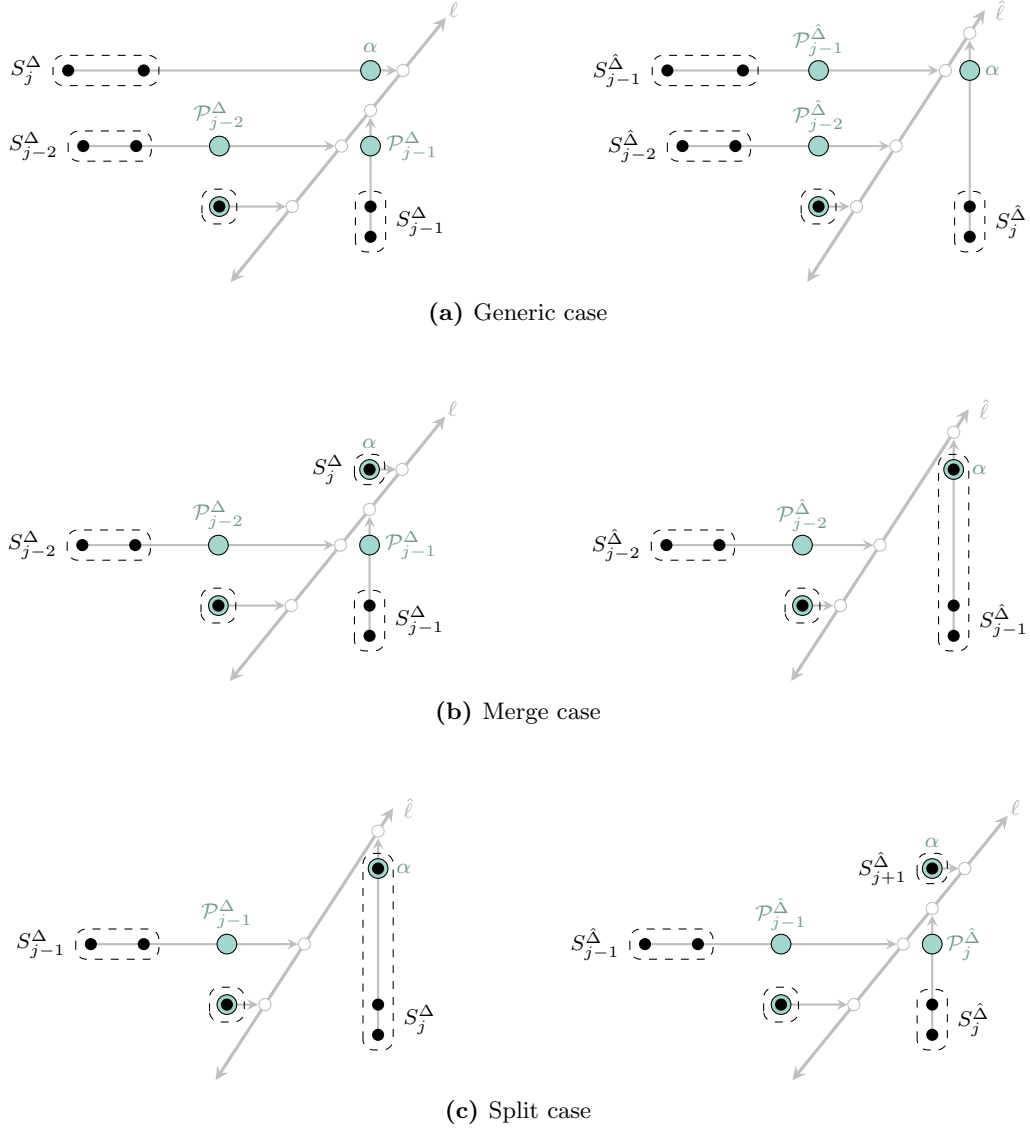


Figure 10: Illustration of how the sets of template points and lift maps change when passing from a cell Δ to an adjacent cell $\hat{\Delta}$, containing the duals of lines ℓ and $\hat{\ell}$, respectively.

(iii) In the split case, we have $|S^{\hat{\Delta}}| = |S^{\Delta}| + 1$ and

$$S_i^{\hat{\Delta}} = \begin{cases} S_i^{\Delta} & \text{if } i < j, \\ S_j^{\Delta} \setminus \{\alpha\} & \text{if } i = j, \\ \{\alpha\} & \text{if } i = j + 1, \\ S_{i-1}^{\Delta} & \text{if } i > j + 1. \end{cases}$$

The next result specifies how the template points and lift maps change as we pass from Δ to $\hat{\Delta}$. To state the result, we let $\mathcal{P}_0^{\Delta} = (-\infty, -\infty)$.

Lemma 5.3.

(i) In the generic case, we have $j > 1$ and

$$\mathcal{P}_i^{\hat{\Delta}} = \begin{cases} \mathcal{P}_i^{\Delta} & \text{if } i \neq j - 1, \\ \max(S_j^{\Delta} \setminus \{\alpha\}) \vee \mathcal{P}_{j-2}^{\Delta} & \text{if } i = j - 1, \end{cases}$$

$$\text{lift}^{\hat{\Delta}}(s) = \begin{cases} \text{lift}^{\Delta}(s) & \text{if } s \notin S_{j-1}^{\Delta} \cup S_j^{\Delta}, \\ \mathcal{P}_j^{\hat{\Delta}} = \alpha & \text{if } s \in S_{j-1}^{\Delta} \cup \{\alpha\}, \\ \mathcal{P}_{j-1}^{\hat{\Delta}} & \text{if } s \in S_j^{\Delta} \setminus \{\alpha\}. \end{cases}$$

(ii) In the merge case, we have

$$\mathcal{P}_i^{\hat{\Delta}} = \begin{cases} \mathcal{P}_i^{\Delta} & \text{if } i < j - 1, \\ \mathcal{P}_{i+1}^{\Delta} & \text{if } i \geq j - 1. \end{cases}$$

$$\text{lift}^{\hat{\Delta}}(s) = \begin{cases} \text{lift}^{\Delta}(s) & \text{if } s \notin S_{j-1}^{\Delta}, \\ \mathcal{P}_{j-1}^{\hat{\Delta}} = \alpha & \text{if } s \in S_{j-1}^{\Delta}. \end{cases}$$

(iii) In the split case, we have

$$\mathcal{P}_i^{\hat{\Delta}} = \begin{cases} \mathcal{P}_i^{\Delta} & \text{if } i < j, \\ \max(S_j^{\Delta} \setminus \{\alpha\}) \vee \mathcal{P}_{j-1}^{\Delta} & \text{if } i = j, \\ \mathcal{P}_{i-1}^{\Delta} & \text{if } i > j. \end{cases}$$

$$\text{lift}^{\hat{\Delta}}(s) = \begin{cases} \text{lift}^{\Delta}(s) & \text{if } s \notin S_j^{\Delta} \setminus \{\alpha\}, \\ \mathcal{P}_j^{\hat{\Delta}} & \text{if } s \in S_j^{\Delta} \setminus \{\alpha\}. \end{cases}$$

Proof. The result follows readily from Lemma 5.2 and the definitions of the sets \mathcal{P}^{Δ} and $\mathcal{P}^{\hat{\Delta}}$. We give the details for case (i); the other cases are similar.

In case (i), if $i \neq j - 1$, then we have

$$\bigcup_{k=1}^i S_k^\Delta = \bigcup_{k=1}^i S_k^{\hat{\Delta}}.$$

Therefore,

$$\mathcal{P}_i^{\hat{\Delta}} = \vee \left(\bigcup_{k=1}^i S_k^{\hat{\Delta}} \right) = \vee \left(\bigcup_{k=1}^i S_k^\Delta \right) = \mathcal{P}_i^\Delta.$$

Moreover, letting $\mathcal{P}_0^{\hat{\Delta}} = (-\infty, -\infty)$, since $S_{j-1}^{\hat{\Delta}} = S_j^\Delta \setminus \{\alpha\}$ and $\mathcal{P}_{j-2}^{\hat{\Delta}} = \mathcal{P}_{j-2}^\Delta$, we have

$$\mathcal{P}_{j-1}^{\hat{\Delta}} = S_{j-1}^{\hat{\Delta}} \vee \mathcal{P}_{j-2}^{\hat{\Delta}} = \max(S_j^\Delta \setminus \{\alpha\}) \vee \mathcal{P}_{j-2}^\Delta.$$

If $i \notin \{j - 1, j\}$, then $S_i^{\hat{\Delta}} = S_i^\Delta$, so for $s \in S_i^\Delta$, we have

$$\text{lift}^{\hat{\Delta}}(s) = \mathcal{P}_i^{\hat{\Delta}} = \mathcal{P}_i^\Delta = \text{lift}^\Delta(s).$$

If $s \in S_{j-1}^\Delta \cup \{\alpha\}$, then $s \in S_j^{\hat{\Delta}}$, so $\text{lift}^{\hat{\Delta}}(s) = \mathcal{P}_j^{\hat{\Delta}}$. Finally, if $s \in S_j^\Delta \setminus \{\alpha\}$, then $s \in S_{j-1}^{\hat{\Delta}}$, so $\text{lift}^{\hat{\Delta}}(s) = \mathcal{P}_{j-1}^{\hat{\Delta}}$. \square

Using Lemma 5.3, it is straightforward to compute $\mathcal{P}^{\hat{\Delta}}$ and $\text{lift}^{\hat{\Delta}}$ by updating \mathcal{P}^Δ and lift^Δ . We discuss some low-level details of this update in Section 5.4.

Lemma 5.3 also immediately implies the following.

Proposition 5.4. *For $s, t \in S$, the following two conditions are equivalent:*

1. $\text{lift}^\Delta(s) < \text{lift}^\Delta(t)$ and $\text{lift}^{\hat{\Delta}}(s) > \text{lift}^{\hat{\Delta}}(t)$
2. $s \in S_{j-1}^\Delta$, $t \in S_j^\Delta \setminus \{\alpha\}$, and $\alpha = s \vee t$.

Note that the equivalent conditions of Proposition 5.4 can hold only in the generic case.

5.3 Permuting Matrices and Updating the RU -Decomposition

Let $\text{rl}(k)$ and $\text{cl}(k)$ denote the k^{th} row and k^{th} column labels of Q , respectively. Then the k^{th} row label of Q^Δ is $\text{lift}^\Delta(\text{rl}(\sigma_\Delta^{-1}(k)))$ and the k^{th} column label of Q^Δ is $\text{lift}^\Delta(\text{cl}(\tau_\Delta^{-1}(k)))$. Changing the row and column labels of Q^Δ by replacing lift^Δ with $\text{lift}^{\hat{\Delta}}$ in these expressions, without changing the underlying matrix, yields a presentation $\tilde{Q}^{\hat{\Delta}}$ of $M^{\hat{\Delta}}$.

Assume that Q^Δ is strongly ordered. Then in the merge and split cases, Lemma 5.3 (ii,iii) imply that $\tilde{Q}^{\hat{\Delta}}$ is also strongly ordered, so we take $Q^{\hat{\Delta}} = \tilde{Q}^{\hat{\Delta}}$ and take the RU -decomposition of $Q^{\hat{\Delta}}$ to be the same as for Q^Δ .

In the generic case, Proposition 5.4 implies that $\tilde{Q}^{\hat{\Delta}}$ is not an ordered presentation. We identify permutation matrices P and P' such that $Q^{\hat{\Delta}} := P\tilde{Q}^{\hat{\Delta}}P'$ is a strongly ordered presentation of $\tilde{Q}^{\hat{\Delta}}$. Specifically, we take P to be the permutation matrix that acts on rows of $\tilde{Q}^{\hat{\Delta}}$ by transposing the block of rows labeled by elements of S_{j-1}^{Δ} with the (adjacent) block of rows labeled by elements of $S_j^{\Delta} \setminus \{\alpha\}$, while fixing the order of rows in each of the two blocks. We take P' to have the analogous action on columns.

To obtain an RU -decomposition of $Q^{\hat{\Delta}}$, we update the RU -decomposition $Q^{\Delta} = R^{\Delta}U^{\Delta}$ by reducing the matrices $\tilde{R} := PR^{\Delta}P'$ and $\tilde{U} := (P')^{-1}U^{\Delta}P'$ as explained in Section 2.3. In principle, any of the update strategies mentioned in Section 2.3 could be used in our setting. Our complexity analysis of barcode template computation in Section 6 considers the standard vineyard update strategy of [44] which, as discussed in Section 2.3, decomposes the permutations represented by P and P' into a sequence of elementary transpositions of adjacent indices, performing a separate RU -update for each transposition. In fact, in the generic setting that the coordinates of the row and column labels of Q are distinct, each of P and P' is either an identity matrix or represents a single transposition of adjacent indices; thus, in this setting, the vineyard strategy and the global RU -update strategy described in Section 2.3 are essentially the same.

The current implementation of barcode template computation in RIVET uses the vineyard strategy, together with some engineering tricks to improve practical performance [79, Sections 8 and 9]. In brief, the code estimates the time required compute the RU -decomposition of $Q^{\hat{\Delta}}$ using vineyard updates, as well as the time required to compute an RU -decomposition of $Q^{\hat{\Delta}}$ from scratch; it then chooses the option estimated to be faster.

Remark 5.5. While the global approach to RU -updates described in Section 2.3 is not implemented in RIVET, this appears to be a promising alternative; it is simpler than what is currently implemented, and it seems likely that it would perform comparably. In future work, it would be interesting to empirically compare these and other RU -update schemes on the problem of barcode template computation.

5.4 Implementation Details

To implement the update procedure described above, when passing from face Δ to face $\hat{\Delta}$ we must update the template points, lift map, and the RU -decomposition. In addition, we must read the barcode template $\mathcal{B}^{\hat{\Delta}}$ from the RU -decomposition $Q^{\hat{\Delta}} = R^{\hat{\Delta}}U^{\hat{\Delta}}$. To do all of this efficiently, we maintain several simple data structures. We now discuss these.

We represent \mathcal{P}^{Δ} as an ordered list. To represent lift^{Δ} in memory, each element $\mathcal{P}_k^{\Delta} \in \mathcal{P}^{\Delta}$ stores its level set $S_k^{\Delta} = (\text{lift}^{\Delta})^{-1}(\mathcal{P}_k^{\Delta})$ again as an ordered list; recall that these level sets form a partition of S . In addition, to enable efficient updates of \mathcal{P}^{Δ} , we maintain a list of A of all anchors, and for each $\alpha \in A$, a pointer to the copy of α in the list representing \mathcal{P}^{Δ} ; if $\alpha \notin \mathcal{P}^{\Delta}$, then this pointer is null. Moreover, each $\alpha \in A$ maintains (possibly null) pointers to the anchors in A immediately below and immediately to the left of α . As we

pass from cell Δ to cell $\hat{\Delta}$ we can update these data structures in constant time using the formulae of Lemma 5.3. We omit the straightforward details.

Following [44], we represent R^Δ and U^Δ in memory by a column-sparse matrix and a row-sparse matrix, respectively; see Section 2.3. To enable efficient computation of the permuted matrices \bar{R} and \bar{U} from R^Δ and U^Δ , each $s \in S$ maintains the minimum and maximum indices of rows k of Q^Δ with $\text{rl}(\sigma_\Delta^{-1}(k)) = s$. (Since Q^Δ is strongly ordered, such rows are ordered consecutively.) Similarly, s also maintains the minimum and maximum indices of columns k of Q^Δ with $\text{cl}(\tau_\Delta^{-1}(k)) = s$. This data allows us to determine in constant time the indices of the blocks of rows and columns that must be exchanged to obtain \bar{R} and \bar{U} from R^Δ and U^Δ .

To efficiently obtain the barcode template $\mathcal{B}^{\hat{\Delta}}$ from the RU -decomposition $Q^{\hat{\Delta}} = R^{\hat{\Delta}}U^{\hat{\Delta}}$, we require that each row and column of $Q^{\hat{\Delta}}$ have access to its label. Since we maintain the map $\text{lift}^{\hat{\Delta}}: S \rightarrow \mathcal{P}^{\hat{\Delta}}$ by storing its level sets, it suffices for each row k of $Q^{\hat{\Delta}}$ to maintain a pointer to $\text{rl}(\sigma_{\hat{\Delta}}^{-1}(k)) \in S$, and similarly for columns. Once initialized at face Δ_0 , these pointers never need to be updated as we traverse the path Γ .

5.5 Computing a Walk Through the Faces

Recall that Δ_0 is the topmost face in $\mathcal{A}(M)$ and that we compute a walk $\Gamma = \Delta_0, \Delta_1, \dots, \Delta_n$ in G which visits each face at least once. We call such a walk *valid*. We now consider the problem of computing a valid walk. Our complexity analysis in Section 6 below holds for any valid walk Γ that traverses each edge of G at most a constant number of times. However, in practice we want to choose Γ to minimize the total cost of RU -updates performed by our algorithm. We describe a simple heuristic for this which treats G as a weighted graph and chooses Γ to be a valid walk of small weight.

We take the weight w_x of an edge $x = [\Delta, \hat{\Delta}]$ in G to be the total number of row and column transpositions required to update a strongly ordered induced presentation Q^Δ of M^Δ to a strongly ordered induced presentation $Q^{\hat{\Delta}}$ of $M^{\hat{\Delta}}$. We regard w_x as a proxy for the work required to obtain an RU -decomposition of $Q^{\hat{\Delta}}$ from one for Q^Δ . It is easily checked that w_x depends only on the line l of $\mathcal{A}(M)$ separating Δ and $\hat{\Delta}$. Moreover, $w_x \neq 0$ only when l^* is the join of incomparable points in s , which corresponds to the generic case of Section 5.2. In this case, to give an explicit formula for w_x , suppose $l^* = \mathcal{P}_j^\Delta$. For $i = 0, 1$, define

$$w_{i,j-1} = \sum_{s \in S_{j-1}^\Delta} \beta_i^M(s), \quad w_{i,j} = \sum_{s \in S_j^\Delta \setminus \{\alpha\}} \beta_i^M(s),$$

Then by Proposition 5.4, $w_x = w_{0,j-1}w_{0,j} + w_{1,j-1}w_{1,j}$.

We would like to choose Γ to be a valid walk of minimum total weight, but computing such a walk is an instance of a classic NP-hard problem and likely itself hard. Therefore, we instead compute a walk Γ whose weight is *approximately* minimum. We mention two classical approximation schemes for this, yielding approximation ratios of 2 and $\frac{3}{2}$, respectively:

Let Γ^* be a valid walk of minimum total weight. For the 2-approximation, we compute a minimum spanning tree \mathcal{M} for G , e.g., via Kruskal’s Algorithm [47]. Depth-first search of \mathcal{M} starting at Δ_0 yields a valid walk Γ in \mathcal{M} traversing each edge of \mathcal{M} at most twice. Since $\text{weight}(\mathcal{M}) \leq \text{weight}(\Gamma^*)$, we have that $\text{weight}(\Gamma) \leq 2 \text{weight}(\Gamma^*)$. Alternatively, [67] shows that a variant of the Christofides $\frac{3}{2}$ -approximation algorithm for the traveling salesman problem on a metric graph [39] yields a valid walk Γ with $\text{weight}(\Gamma) \leq \frac{3}{2} \text{weight}(\Gamma^*)$.

6 Complexity of Computing the Augmented Arrangement

We now turn to the proof of Theorem 1.2 (ii), which bounds the time and memory cost of our algorithm for computing the augmented arrangement $\mathcal{A}^\bullet(M)$.

Proof of Theorem 1.2 (ii). Recall that computing $\mathcal{A}^\bullet(M)$ entails computing the anchors, the line arrangement $\mathcal{A}(M)$, the point location data structure, and the barcode templates. To prove Theorem 1.2 (ii), we analyze the cost of each of these steps. Table 1 summarizes the cost of each step.

Computation	Time	Memory
Set of anchors of M	$O(\kappa)$	$O(\kappa)$
Line arrangement and data structure for point location	$O(\kappa^2 \log \kappa)$	$O(\kappa^2)$
Barcode templates	$O(m^3 \kappa + \kappa^2(m + \log \kappa))$	$O(m^2 + m\kappa^2)$

Table 1: Cost of augmented arrangement sub-computations

As noted at the beginning of Section 5, computing the set of anchors requires $O(\kappa)$ time and $O(\kappa)$ memory. Recall from Section 2.4 that the Bentley-Ottmann algorithm [52] computes a line arrangement with l lines and v vertices in $O((l+v) \log l)$ time and $O(l+v)$ memory. Moreover, for e the number of edges in the arrangement, we can compute a point location data structure for the arrangement in $O(e \log e)$ time and $O(e)$ memory. As mentioned in Section 3.1, $\mathcal{A}(M)$ has $O(\kappa)$ lines, $O(\kappa^2)$ vertices, and $O(\kappa^2)$ edges. Thus, computing $\mathcal{A}(M)$ via Bentley-Ottmann requires $O(\kappa^2 \log \kappa)$ time and $O(\kappa^2)$ memory, and a point location data structure for $\mathcal{A}(M)$ can be computed in $O(\kappa^2 \log \kappa)$ time and $O(\kappa^2)$ memory.¹

The substeps involved in the computation of the barcode templates are listed in Table 2, together with their runtimes. We now discuss the cost of each substep.

¹As noted in Section 2.4, there exist algorithms for computing line arrangements that are asymptotically faster than Bentley-Ottman. However, since computing the point location data structure takes $O(\kappa^2 \log \kappa)$ time, Bentley-Ottmann is not a bottleneck in the time complexity of our query scheme.

Computation	Time
Walk Γ (via the 2-approximation algorithm for the optimal walk, using Kruskal's MST algorithm)	$O(\kappa^2 \log \kappa)$
\mathcal{P}^{Δ_0} and lift^{Δ_0}	$O(m \log m)$
RU -decomposition at Δ_0	$O(m^3)$
updates to \mathcal{P}^Δ and lift^Δ	$O(\kappa^2)$
updates to permutations and RU -decompositions	$O(m^3 \kappa)$
reading barcode templates	$O(m \kappa^2)$

Table 2: Cost of barcode template sub-computations

On a graph with E edges and V vertices, Kruskal's algorithm runs in time $O(E \log V)$. As noted in Section 3.1, the numbers of vertices, edges, and faces in \mathcal{A} are each $O(\kappa^2)$. By duality, G also has $O(\kappa^2)$ vertices and edges. Thus, the runtime of Kruskal's algorithm on G is $O(\kappa^2 \log \kappa)$, and the runtime of depth-first search on the resulting spanning tree is $O(\kappa^2)$. Hence, the cost of computing Γ using the approach based on Kruskal's algorithm described at end of Section 5.1 is $O(\kappa^2 \log \kappa)$.

Recall that to compute the RU -decomposition and barcode templates at the initial cell Δ_0 , we first compute the map lift^{Δ_0} and the ordered presentation Q^{Δ_0} . As explained in Section 5.1, these computations are simple applications of sorting; they require time $O(m \log m)$. Computing the RU -decomposition of Q^{Δ_0} , and hence the barcode template \mathcal{B}^{Δ_0} , then requires $O(m^3)$ time.

We now analyze the cost of performing the updates at each cell Δ_i for $i > 0$. As we move from cell Δ to cell $\hat{\Delta}$, we can update both \mathcal{P}^Δ and lift^Δ , as well as the associated pointers described in Section 5.4, in constant time. Since the walk Γ has length $O(\kappa^2)$, the total cost of all such updates is $O(\kappa^2)$.

For our cost analysis of permuting the matrices and updating the RU -decompositions, we consider only the vineyard update strategy of [44]. We will show that for this strategy, the total cost of permuting the matrices and updating the RU -decompositions is $O(m^3 \kappa)$. To do so, we count the number of transpositions involving a pair of rows of Q with given labels a and b . These rows can swap only if a and b are incomparable, and they swap only when crossing the line dual to this anchor. As we traverse Γ , each anchor line is crossed $O(\kappa)$ times. There are at most $O(m^2)$ label pairs, so at most $O(m^2 \kappa)$ row transpositions are performed in total. The same analysis applies to the column transpositions. By the results of [44], if the row transpositions of R and column transpositions of U are performed implicitly, then the RU -update corresponding to each row or column transposition requires $O(m)$ time. Thus, the total cost of all permutations and RU -updates is $O(m^3 \kappa)$. Reading a barcode template from the RU -decomposition requires $O(m)$ time. Therefore, the total cost of reading all barcode templates is $O(m \kappa^2)$.

The memory cost of computing all barcode templates is dominated by the cost of storing a presentation matrix, which is $O(m^2)$, and the cost of storing the output, which is $O(m\kappa^2)$. Thus, computing all barcode templates requires $O(m^3\kappa + \kappa^2(m + \log \kappa))$ time and $O(m^2 + m\kappa^2)$ memory. Theorem 1.2 (ii) now follows. \square

Acknowledgments

This work was funded in part by NSF grant DMS-1606967 and a grant from the Simons Foundation (Award ID 963845). We thank our collaborators on the RIVET software, especially Anway De, Bryn Keller, Simon Segert, Alex Yu, and Roy Zhao. Our joint work on RIVET has helped shape our understanding of the ideas in this paper. We also thank the anonymous reviewers of [79] for helpful feedback on that work, which has impacted the writing here.

References

- [1] Á. J. Alonso. A sparse multicover bifiltration of linear size. In *41st International Symposium on Computational Geometry (SoCG 2025)*, pages 6–1. Schloss Dagstuhl–Leibniz-Zentrum für Informatik, 2025.
- [2] Á. J. Alonso and M. Kerber. Decomposition of zero-dimensional persistence modules via rooted subsets. *Discrete & Computational Geometry*, pages 1–21, 2024.
- [3] Á. J. Alonso, M. Kerber, T. Lam, and M. Lesnick. Delaunay bifiltrations of functions on point clouds. In *Proceedings of the 2024 Annual ACM-SIAM Symposium on Discrete Algorithms (SODA)*, pages 4872–4891. SIAM, 2024.
- [4] Á. J. Alonso, M. Kerber, and S. Pritam. Filtration-domination in bifiltered graphs. In *2023 proceedings of the symposium on algorithm engineering and experiments (ALENEX)*, pages 27–38. SIAM, 2023.
- [5] G. Azumaya. Corrections and supplementaries to my paper concerning krull-remak-schmidt’s theorem. *Nagoya mathematical journal*, 1:117–124, 1950.
- [6] U. Bauer, F. Lenzen, and M. Lesnick. Efficient Two-Parameter Persistence Computation via Cohomology. In E. W. Chambers and J. Gudmundsson, editors, *39th International Symposium on Computational Geometry (SoCG 2023)*, volume 258 of *Leibniz International Proceedings in Informatics (LIPIcs)*, pages 15:1–15:17, Dagstuhl, Germany, 2023. Schloss Dagstuhl – Leibniz-Zentrum für Informatik.
- [7] U. Bauer and L. Scoccola. Multi-parameter persistence modules are generically indecomposable. *International Mathematics Research Notices*, 2025(5), 2025.
- [8] K. Benjamin, A. Bhandari, J. D. Kepple, R. Qi, Z. Shang, Y. Xing, Y. An, N. Zhang, Y. Hou, T. L. Crockford, et al. Multiscale topology classifies cells in subcellular spatial transcriptomics. *Nature*, 630(8018):943–949, 2024.
- [9] S. Biasotti, A. Cerri, P. Frosini, and D. Giorgi. A new algorithm for computing the 2-dimensional matching distance between size functions. *Pattern Recognition Letters*, 32(14):1735–1746, 2011.

- [10] H. B. Bjerkevik. Stabilizing decomposition of multiparameter persistence modules. *Foundations of Computational Mathematics*, pages 1–60, 2025.
- [11] H. B. Bjerkevik and M. Kerber. Asymptotic improvements on the exact matching distance for 2-parameter persistence. *Journal of Computational Geometry*, 14(1):309–342, 2023.
- [12] B. Blanchette, T. Brüstle, and E. J. Hanson. Exact structures for persistence modules. *arXiv preprint arXiv:2308.01790*, 2023.
- [13] B. Blanchette, T. Brüstle, and E. J. Hanson. Homological approximations in persistence theory. *Canadian Journal of Mathematics*, page 1–38, 2022.
- [14] N. Blaser, M. Brun, O. H. Gardaa, and L. M. Salbu. Core bifiltration. *arXiv preprint arXiv:2405.01214*, 2024.
- [15] A. J. Blumberg and M. Lesnick. Stability of 2-parameter persistent homology. *Foundations of Computational Mathematics*, 24(2):385–427, 2024.
- [16] J.-D. Boissonnat, F. Chazal, and M. Yvinec. *Geometric and topological inference*, volume 57. Cambridge University Press, 2018.
- [17] M. Botnan and W. Crawley-Boevey. Decomposition of persistence modules. *Proceedings of the American Mathematical Society*, 148(11):4581–4596, 2020.
- [18] M. Botnan and M. Lesnick. An introduction to multiparameter persistence. In *Representations of Algebras and Related Structures: International Conference on Representations of Algebras, ICRA 2020, 9–25 November 2020*, pages 77–150. EMS Press, 2023.
- [19] M. B. Botnan, S. Oppermann, and S. Oudot. Signed barcodes for multi-parameter persistence via rank decompositions and rank-exact resolutions. *Foundations of Computational Mathematics*, pages 1–60, 2024.
- [20] M. B. Botnan, S. Oppermann, S. Oudot, and L. Scoccola. On the bottleneck stability of rank decompositions of multi-parameter persistence modules. *Advances in Mathematics*, 451:109780, 2024.
- [21] M. Buchet, B. B. Dornelas, and M. Kerber. Sparse higher order čech filtrations. *Journal of the ACM*, 71(4):1–23, 2024.
- [22] O. Busaryev, T. K. Dey, and Y. Wang. Tracking a generator by persistence. *Discrete Mathematics, Algorithms and Applications*, 2(04):539–552, 2010.
- [23] C. Cai, W. Kim, F. Mémoli, and Y. Wang. Elder-rule-staircodes for augmented metric spaces. *SIAM Journal on Applied Algebra and Geometry*, 5(3):417–454, 2021.
- [24] G. Carlsson. Topology and data. *American Mathematical Society*, 46(2):255–308, 2009.
- [25] G. Carlsson and F. Mémoli. Multiparameter hierarchical clustering methods. *Classification as a Tool for Research*, pages 63–70, 2010.
- [26] G. Carlsson, G. Singh, and A. Zomorodian. Computing multidimensional persistence. *Algorithms and Computation*, pages 730–739, 2009.
- [27] G. Carlsson and M. Vejdemo-Johansson. *Topological data analysis with applications*. Cambridge University Press, 2021.

- [28] G. Carlsson and A. Zomorodian. The theory of multidimensional persistence. *Discrete and Computational Geometry*, 42(1):71–93, 2009.
- [29] M. Carriere and A. Blumberg. Multiparameter persistence image for topological machine learning. *Advances in Neural Information Processing Systems*, 33:22432–22444, 2020.
- [30] A. Cerri, B. Di Fabio, M. Ferri, P. Frosini, and C. Landi. Betti numbers in multidimensional persistent homology are stable functions. *Mathematical Methods in the Applied Sciences*, 36(12):1543–1557, 2013.
- [31] W. Chachólski, A. Guidolin, I. Ren, M. Scolamiero, and F. Tombari. Koszul complexes and relative homological algebra of functors over posets. *Foundations of Computational Mathematics*, pages 1–45, 2024.
- [32] W. Chachólski, M. Scolamiero, and F. Vaccarino. Combinatorial presentation of multidimensional persistent homology. *Journal of Pure and Applied Algebra*, 221(5):1055–1075, 2017.
- [33] F. Chazal, D. Cohen-Steiner, and Q. Mérigot. Geometric inference for probability measures. *Foundations of Computational Mathematics*, pages 1–19, 2011.
- [34] F. Chazal and B. Michel. An introduction to topological data analysis: fundamental and practical aspects for data scientists. *Frontiers in artificial intelligence*, 4:667963, 2021.
- [35] B. Chazelle and H. Edelsbrunner. An optimal algorithm for intersecting line segments in the plane. *J. ACM*, 39(1):1–54, 1992.
- [36] Y. Chen, I. Segovia-Dominguez, C. G. Akcora, Z. Zhen, M. Kantarcioglu, Y. Gel, and B. Coskunuzer. Emp: Effective multidimensional persistence for graph representation learning. In *Learning on Graphs Conference*, pages 24–1. PMLR, 2024.
- [37] Y. Chen, I. Segovia-Dominguez, B. Coskunuzer, and Y. Gel. Tamp-s2gcnets: coupling time-aware multipersistence knowledge representation with spatio-supra graph convolutional networks for time-series forecasting. In *International conference on learning representations*, 2022.
- [38] X. Cheng, S. Mukherjee, S. Samaga, and T. K. Dey. Gril: A 2-parameter persistence based vectorization for machine learning. In *Proc. ICML 2023 workshop TAGML*, 2023.
- [39] N. Christofides. Worst-case analysis of a new heuristic for the travelling salesman problem. *Report 388, Graduate School of Industrial Administration, CMU*, 1976.
- [40] Y.-M. Chung, S. Day, and C.-S. Hu. A multi-parameter persistence framework for mathematical morphology. *Scientific reports*, 12(1):6427, 2022.
- [41] Y.-M. Chung, C.-S. Hu, E. Sun, and H. C. Tseng. Morphological multiparameter filtration and persistent homology in mitochondrial image analysis. *Plos one*, 19(9):e0310157, 2024.
- [42] N. Clause, T. K. Dey, F. Mémoli, and B. Wang. Meta-diagrams for 2-parameter persistence. *Discrete & Computational Geometry*, pages 1–27, 2025.
- [43] D. Cohen-Steiner, H. Edelsbrunner, and J. Harer. Stability of persistence diagrams. *Discrete and Computational Geometry*, 37(1):103–120, 2007.

- [44] D. Cohen-Steiner, H. Edelsbrunner, and D. Morozov. Vines and vineyards by updating persistence in linear time. In *Proceedings of the twenty-second annual symposium on Computational geometry*, pages 119–126. ACM, 2006.
- [45] R. Corbet, U. Fugacci, M. Kerber, C. Landi, and B. Wang. A kernel for multi-parameter persistent homology. *Computers & graphics: X*, 2:100005, 2019.
- [46] R. Corbet, M. Kerber, M. Lesnick, and G. Osang. Computing the multicover bifiltration. *Discrete & Computational Geometry*, 70(2):376–405, 2023.
- [47] T. Cormen, C. Leiserson, R. Rivest, and C. Stein. *Introduction to Algorithms*. MIT Press, 2009.
- [48] B. Coskunuzer, I. Segovia-Dominguez, Y. Chen, and Y. R. Gel. Time-aware knowledge representations of dynamic objects with multidimensional persistence. In *Proceedings of the AAAI Conference on Artificial Intelligence*, volume 38, pages 11678–11686, 2024.
- [49] D. Cox, J. Little, and D. O’Shea. *Using algebraic geometry*, volume 185. Springer Verlag, 1998.
- [50] W. Crawley-Boevey. Decomposition of pointwise finite-dimensional persistence modules. *Journal of Algebra and Its Applications*, 14(05):1550066, 2015.
- [51] A. De, T. Vo, and M. Wright. Value-offset bifiltrations for digital images. *Computational Geometry*, 109:101939, 2023.
- [52] M. de Berg, O. Cheong, M. van Kreveld, and M. Overmars. *Computational Geometry: Algorithms and Applications*. Springer, 2008.
- [53] A. Demir, B. Coskunuzer, Y. Gel, I. Segovia-Dominguez, Y. Chen, and B. Kiziltan. Todd: Topological compound fingerprinting in computer-aided drug discovery. *Advances in Neural Information Processing Systems*, 35:27978–27993, 2022.
- [54] T. K. Dey, J. Jendrysiak, and M. Kerber. Decomposing multiparameter persistence modules. In *41st International Symposium on Computational Geometry (SoCG 2025)*, pages 41–1. Schloss Dagstuhl–Leibniz-Zentrum für Informatik, 2025.
- [55] T. K. Dey and Y. Wang. *Computational topology for data analysis*. Cambridge University Press, 2022.
- [56] T. K. Dey and C. Xin. Generalized persistence algorithm for decomposing multiparameter persistence modules. *Journal of Applied and Computational Topology*, 2022.
- [57] H. Edelsbrunner and J. Harer. *Computational topology: an introduction*. American Mathematical Society, 2010.
- [58] H. Edelsbrunner, D. Letscher, and A. Zomorodian. Topological persistence and simplification. *Discrete and Computational Geometry*, 28(4):511–533, 2002.
- [59] H. Edelsbrunner and G. Osang. The multi-cover persistence of euclidean balls. *Discrete & Computational Geometry*, 65:1296–1313, 2021.
- [60] H. Edelsbrunner and G. Osang. A simple algorithm for higher-order delaunay mosaics and alpha shapes. *Algorithmica*, 85(1):277–295, 2023.

- [61] A. Fernandes, S. Oudot, and F. Petit. Computation of gamma-linear projected barcodes for multi-parameter persistence. *Journal of Applied and Computational Topology*, 9(2):12, 2025.
- [62] P. Frosini and M. Mulazzani. Size homotopy groups for computation of natural size distances. *Bulletin of the Belgian Mathematical Society Simon Stevin*, 6(3):455–464, 1999.
- [63] U. Fugacci, M. Kerber, and A. Rolle. Compression for 2-parameter persistent homology. *Computational Geometry*, 109:101940, 2023.
- [64] B. Giunti, J. Lazovskis, and B. Rieck. DONUT: Database of Original & Non-Theoretical Uses of Topology, 2022. <https://donut.topology.rocks>.
- [65] N. Hellmer and J. Spaliński. Density sensitive bifiltered dower complexes via total weight. *arXiv preprint arXiv:2405.15592*, 2024.
- [66] A. Hickok. Computing persistence diagram bundles. *arXiv preprint arXiv:2210.06424*, 2022.
- [67] J. Hoogeveen. Analysis of christofides’ heuristic: Some paths are more difficult than cycles. *Operations Research Letters*, 10(5):291–295, 1991.
- [68] M. Kerber, M. Lesnick, and S. Oudot. Exact Computation of the Matching Distance on 2-Parameter Persistence Modules. In G. Barequet and Y. Wang, editors, *35th International Symposium on Computational Geometry (SoCG 2019)*, volume 129 of *Leibniz International Proceedings in Informatics (LIPIcs)*, pages 46:1–46:15, Dagstuhl, Germany, 2019. Schloss Dagstuhl – Leibniz-Zentrum für Informatik.
- [69] M. Kerber and A. Rolle. *Fast Minimal Presentations of Bi-graded Persistence Modules*, pages 207–220. SIAM, 2021.
- [70] D. Kim, W. Kim, and W. Lee. Super-Polynomial Growth of the Generalized Persistence Diagram. In O. Aichholzer and H. Wang, editors, *41st International Symposium on Computational Geometry (SoCG 2025)*, volume 332 of *Leibniz International Proceedings in Informatics (LIPIcs)*, pages 64:1–64:20, Dagstuhl, Germany, 2025. Schloss Dagstuhl – Leibniz-Zentrum für Informatik.
- [71] W. Kim and F. Mémoli. Generalized persistence diagrams for persistence modules over posets. *Journal of Applied and Computational Topology*, 5(4):533–581, 2021.
- [72] M. Kreuzer and L. Robbiano. Computational commutative algebra 1. *Month*, 2000.
- [73] M. Kreuzer and L. Robbiano. *Computational commutative algebra 2*, volume 1. Springer, 2005.
- [74] R. La Scala and M. Stillman. Strategies for computing minimal free resolutions. *Journal of Symbolic Computation*, 26(4):409–431, 1998.
- [75] C. Landi. The rank invariant stability via interleavings. *Research in Computational Topology*, 13:1, 2018.
- [76] M. Lesnick. The theory of the interleaving distance on multidimensional persistence modules. *Foundations of Computational Mathematics*, 15(3):613–650, 2015.
- [77] M. Lesnick and K. McCabe. Nerve models of subdivision bifiltrations. *arXiv preprint arXiv:2406.07679*, 2024.

- [78] M. Lesnick and K. McCabe. Sparse approximation of the subdivision-rips bifiltration for doubling metrics. *arXiv preprint arXiv:2408.16716*, 2024.
- [79] M. Lesnick and M. Wright. Interactive visualization of 2-d persistence modules. *arXiv preprint arXiv:1512.00180*, 2015.
- [80] M. Lesnick and M. Wright. Computing minimal presentations and bigraded betti numbers of 2-parameter persistent homology. *SIAM Journal on Applied Algebra and Geometry*, 6(2):267–298, 2022.
- [81] D. Loiseaux, M. Carrière, and A. Blumberg. A framework for fast and stable representations of multiparameter persistent homology decompositions. *Advances in Neural Information Processing Systems*, 36:35774–35798, 2023.
- [82] D. Loiseaux, M. Carrière, and A. J. Blumberg. Multi-parameter module approximation: an efficient and interpretable invariant for multi-parameter persistence modules with guarantees. *Journal of Applied and Computational Topology*, 9(4):1–60, 2025.
- [83] D. Loiseaux and H. Schreiber. multipers: Multiparameter persistence for machine learning. *Journal of Open Source Software*, 9(103):6773, 2024.
- [84] D. Loiseaux, L. Scoccola, M. Carrière, M. B. Botnan, and S. Oudot. Stable vectorization of multi-parameter persistent homology using signed barcodes as measures. *Advances in Neural Information Processing Systems*, 36:68316–68342, 2023.
- [85] Y. Luo and B. J. Nelson. Accelerating iterated persistent homology computations with warm starts. *Computational Geometry*, 120:102089, 2024.
- [86] D. Morozov and A. Patel. Output-sensitive computation of generalized persistence diagrams for 2-filtrations. *arXiv preprint arXiv:2112.03980*, 2021.
- [87] D. Morozov and L. Scoccola. Computing betti tables and minimal presentations of zero-dimensional persistent homology. In *41st International Symposium on Computational Geometry (SoCG 2025)*, pages 69–1. Schloss Dagstuhl–Leibniz-Zentrum für Informatik, 2025.
- [88] S. Oudot and L. Scoccola. On the stability of multigraded betti numbers and hilbert functions. *SIAM Journal on Applied Algebra and Geometry*, 8(1):54–88, 2024.
- [89] S. Y. Oudot. *Persistence theory: from quiver representations to data analysis*, volume 209. American Mathematical Society Providence, 2015.
- [90] A. Patel. Generalized persistence diagrams. *Journal of Applied and Computational Topology*, 1(3):397–419, 2018.
- [91] I. Peeva. *Graded Syzygies*. Springer, 2011.
- [92] M. Piekenbrock and J. Perea. Move schedules: fast persistence computations in coarse dynamic settings. *Journal of Applied and Computational Topology*, 8:301–345, 2024.
- [93] F. P. Preparata and M. I. Shamos. *Computational geometry: an introduction*. Springer Science & Business Media, 2012.
- [94] R. Rabadán and A. J. Blumberg. *Topological data analysis for genomics and evolution: topology in biology*. Cambridge University Press, 2019.

- [95] E. Riehl. *Category Theory in Context*. Dover Publications, 2016.
- [96] Y. Schiff, P. Das, E. Vijil, and K. N. Ramamurthy. Characterizing the latent space of molecular deep generative models with persistent homology metrics. In *TDA & Beyond Workshop, Annual Conference on Neural Information Processing Systems*, 2020.
- [97] L. Scoccola and A. Rolle. Persistable: persistent and stable clustering. *Journal of Open Source Software*, 8(83):5022, 2023.
- [98] L. Scoccola, S. Setlur, D. Loiseaux, M. Carrière, and S. Oudot. Differentiability and optimization of multiparameter persistent homology. In R. Salakhutdinov, Z. Kolter, K. Heller, A. Weller, N. Oliver, J. Scarlett, and F. Berkenkamp, editors, *Proceedings of the 41st International Conference on Machine Learning*, volume 235 of *Proceedings of Machine Learning Research*, pages 43986–44011. PMLR, 21–27 Jul 2024.
- [99] D. R. Sheehy. A multicover nerve for geometric inference. In *CCCG*, pages 309–314, 2012.
- [100] The RIVET Developers. Rivet. <https://github.com/rivetTDA/rivet/>, 2020. Version 1.1.0.
- [101] C. D. Toth, J. O’Rourke, and J. E. Goodman. *Handbook of discrete and computational geometry*. CRC press, 3rd edition, 2017.
- [102] O. Vipond. Multiparameter persistence landscapes. *Journal of Machine Learning Research*, 21(61):1–38, 2020.
- [103] O. Vipond, J. A. Bull, P. S. Macklin, U. Tillmann, C. W. Pugh, H. M. Byrne, and H. A. Harrington. Multiparameter persistent homology landscapes identify immune cell spatial patterns in tumors. *Proceedings of the National Academy of Sciences*, 118(41):e2102166118, 2021.
- [104] L. Wasserman. Topological data analysis. *Annual review of statistics and its application*, 5(2018):501–532, 2018.
- [105] M. Wright and X. Zheng. Topological data analysis on simple english wikipedia articles. *The PUMP Journal of Undergraduate Research*, 3:308–328, Dec. 2020.
- [106] K. Xia and G.-W. Wei. Multidimensional persistence in biomolecular data. *Journal of computational chemistry*, 36(20):1502–1520, 2015.
- [107] L. Xian, H. Adams, C. M. Topaz, and L. Ziegelmeier. Capturing dynamics of time-varying data via topology. *Foundations of Data Science*, 4(1):1–36, 2022.
- [108] Y. Zhang, C. Shen, and K. Xia. Multi-cover persistence (mcp)-based machine learning for polymer property prediction. *Briefings in Bioinformatics*, 25(6), 2024.
- [109] A. Zomorodian and G. Carlsson. Computing persistent homology. *Discrete and Computational Geometry*, 33(2):249–274, 2005.